Netherlands Environmental Assessment Agency

MNP report 555034002/2007

Monitoring aerosol over Europe using AATSR
HIRAM final report

R.B.A. Koelemeijer, M. Schaap*,
R.M.A. Timmermans*, T. van Noije,
J. Matthijsen, P.J.H. Builtjes*,
R. Schoemaker**, G. de Leeuw**

* TNO Bouw en Ondergrond
** TNO Defensie en Veiligheid

Contact:
Robert Koelemeijer
Milieu- en Natuurplanbureau (MNP)
Luchtkwaliteit en Europese Duurzaamheid
Robert.Koelemeijer@mnp.nl

This investigation has been funded in part by the Netherlands Agency for Aerospace Programmes (NIVR), within the framework of project E/555034/02, HIRAM, NIVR project code 53516 RI.

Netherlands Environmental Assessment Agency (MNP), P.O. Box 303, 3720 AH Bilthoven,
telephone: +31 30 274 2745; www.mnp.nl

Rapport in het kort

Monitoring van aerosol in Europa met AATSR

HIRAM-eindrapport

Fijnstofconcentraties zijn moeilijk vergelijkbaar tussen verschillende EU-lidstaten omdat verschillende meetmethoden worden gehanteerd. In dit rapport is onderzocht of satellietmetingen (AATSR) kunnen worden gebruikt om fijnstofconcentraties op Europese schaal beter in kaart te brengen. Het is daarmee een vervolg op het PARMA-project, waarin een vergelijkbare studie is gedaan met behulp van MODIS-satellietgegevens. De AATSR-gegevens uit 2003 bleken echter van mindere goede kwaliteit dan de MODIS-gegevens. De belangrijkste foutenbron in de AATSR-gegevens is gerelateerd aan het niet voldoende detecteren van bewolking, waardoor de hoeveelheid aerosol abusievelijk te hoog wordt gemeten. Het verbeteren van de wolkendetectie in AATSR is nodig voordat deze gegevens kunnen worden toegepast voor het verbeteren van fijnstofkaarten.

Trefwoorden: data-assimilatie, optische dikte, fijn stof, AATSR

Contents

Summary

Both for the assessment of exposure of the population to particulate matter (PM) and for the assessment of climate forcing by aerosols, it is mandatory to reduce the uncertainties concerning aerosol or particulate matter abundances. At present all EU member states perform air quality measurements, but the diversity and quality of the ground network hampers a comparison of absolute PM levels across member states. Satellite measurements are less precise than ground based measurements, but they have the advantage that they provide full spatial coverage and are – in principle – consistent for the whole European region. This suggests that satellite measurements may be useful to improve the insight in aerosol distributions in Europe in combination with models and ground based measurements. Indeed, in the PARMA project (Monitoring **Par**ticulate **Ma**tter for Climate and Health Effects in Europe), carried out by MNP and TNO in the period 2004-2006 (Koelemeijer et al., 2006a), it was shown that adding satellite information from the Moderate Resolution Imaging Spectroradiometer (MODIS) to modelled fields and ground based measurements leads to a better description of PM distributions in Europe. This report presents the final results of the HIRAM project (**Hi**gh-**R**esolution **A**ir quality **M**onitoring over Europe). In this project the use of satellite data from the Advanced Along-Track Scanning Radiometer (AATSR) instrument (on board ENVISAT) is investigated. The results of this project are therefore complementary to the PARMA study. The results are presented along the following lines:

- Validation of AATSR data;
- Mapping of $PM_{2.5}$ using the AATSR data;
- Radiative forcing of nitrate and sulphate based on simulations.

Validation of AATSR by comparison to AERONET and MODIS
In the project the validation of data from the AATSR received extra attention, by using independent AERONET ground based observations of aerosol optical thickness (AOT), and by comparison with MODIS data. In this study, a one-year dataset of AATSR aerosol optical thickness data over Europe has been processed for the first time. Because of the large data volume, it was decided to make the cloud detection part of the retrieval algorithm fully automatic. However, without rigorous cloud-screening, the large scale distribution of AOT from AATSR in 2003 appeared to be unrealistic. Also, large point sources or source areas such as major cities and even larger scale hot-spot regions could barely be detected. Comparison with MODIS yearly average AOT in 2003, as well as ATSR-2 data revealed large differences in spatial distribution of the AOT. It was found that the time correlation between AERONET and AATSR, averaged over all stations, was 0.53 (0.59 median), while it was 0.65 (0.73 median) using MODIS data. Largest errors in AATSR were found in Northern and Eastern Europe, and are likely related to undetected clouds or insufficient surface correction in cases with snow or ice cover. The spatial correlation between yearly average AOT values from AATSR and AERONET was much lower than that using MODIS data. The validation also showed that AATSR has almost no bias, while MODIS did show a significant bias against AERONET. However, it was shown in the PARMA study that the bias in MODIS has a clear seasonality, and could be largely corrected for in a straightforward manner. Nevertheless, the reasons for the bias and its seasonal behaviour have not yet been fully elaborated and understood.

In this project, it was found that about 50% of the AATSR data in 2003 need to be discarded from further use because of potential contamination by clouds or by insufficient surface correction in cases with snow or ice cover. For MODIS about 33% of the data is potentially contaminated by clouds or snow. In the case of AATSR, contamination of the retrieved AOT by clouds and snow-coverage is the dominating source of error. The main conclusion is that the detection of clouds and snow-coverage needs to be improved before the AATSR retrieval method can be used in a non-supervised mode for air quality studies in Europe. Besides, the lower accuracy as compared to MODIS, also the number of AATSR observations is much more limited because of the small swath width. It turns out that in practice about 65 AATSR observations are available per year for a given location, while MODIS (Terra and Aqua combined) has about 240 observations per year for a given location.

Results of the $PM_{2.5}$ mapping experiments

Similar to the PARMA project, two different approaches were followed to use satellite AOT data for $PM_{2.5}$ mapping: a statistical approach and a data-assimilation approach. In an attempt to avoid the large problems with cloud (and snow/ice) contamination in the AATSR data, a selection criterion was used for additional cloud-screening, based on monthly average data. This screened dataset was used for the statistical approach to map $PM_{2.5}$. Visual inspection shows that this leads to better performance for Northern Europe and better agreement with the results from the PARMA study. In the assimilation approach used to map $PM_{2.5}$, instantaneous data are used and a similar cloud-screening method, based on monthly average data, was not possible. Therefore we have used the MODIS cloud detection in an attempt to avoid cloud contamination in AATSR.

The spatial correlation coefficient between the yearly AOT retrieved from AATSR and the yearly average AOT_F from MODIS is 0.58, after additional cloud screening of the AATSR data. This indicates that these satellite instruments still show substantial differences in aerosol optical thickness distributions. Since the statistical mapping approach is based on both model calculations and measurements, the resulting $PM_{2.5}$ maps based on AATSR and MODIS differs less than the AOT fields. Therefore, the results of the statistical mapping approach were to some extent comparable to MODIS, after application of an additional cloud-screening of the AATSR data. However, there are reasons suggesting that the MODIS based map, resulting from the PARMA study, is more realistic than the map based on AATSR, presented in this report. First, bias-corrected MODIS data show a better comparison with independent AOT measurements from AERONET, as compared to AATSR versus AERONET. Second, the fitted $PM_{2.5}$ map based on MODIS exhibits smaller residuals when compared with $PM_{2.5}$ measurements from AirBase. Third, the MODIS results are less sensitive to more-or-less arbitrary methodological choices.

Similar to the conclusion of the PARMA study, the assimilation leads to higher $PM_{2.5}$ concentrations compared to the free model run, as the model underestimates the AOT. For a discussion on these issues we refer to the PARMA report. The limited amount of AATSR data for the months June and July 2003 have, when assimilated, a limited influence on the modelled $PM_{2.5}$ fields. In other words, the AATSR data do not strongly constrain the model in the assimilation.

Radiative forcing of nitrate compared to sulphate

In this study, also aerosol radiative forcing aspects were investigated. Based on our simulations for 2003, the annual radiative forcing by nitrate is calculated to be in the order of 55% of that by sulphate, whereas for 1995 the percentage was only 20% (Schaap, 2003). In

summer, nitrate is found to be only regionally important, e.g. in Northwestern Europe, where the forcing of nitrate equals that by sulphate. In the winter the nitrate forcing over Europe is about equal to the sulphate forcing. These results are in agreement with estimates based on measured data (Ten Brink et al., 1997; Schaap et al., 2002). It is concluded that nitrate forcing is significant and gaining importance compared to sulphate and should thus be taken into account to estimate the impact of regional climate change in Europe.

1. Introduction

Particulate matter (PM) is a major environmental factor affecting public health in Europe. Even today, in Europe still some 35% of the urban population is exposed to PM_{10} concentrations above EU limit values (EEA, 2004). In the past decades, many studies have identified and quantified health effects of short-term exposure to particulate matter (e.g., Brunekreef and Holgate, 2002; Knol and Staatsen, 2005). Effects of long-term exposure to particulate matter are much more uncertain than the short-term effects, but are believed to have a much greater effect on health loss (Dockery et al., 1993; Pope et al., 1995; 2002). Within the EU's Clean Air For Europe programme (CAFE), a health assessment was made of long-term exposure to particulate matter. In that assessment, it was concluded that currently in the EU there is a loss in statistical life expectancy of over 8 months due to $PM_{2.5}$ in air, equivalent to 3.6 million life years lost annually (EU, 2005).

Aerosols also affect the environment by modifying the radiative budget of the Earth (direct and indirect radiative forcing). Recent estimates of direct radiative forcing by reflective aerosols (like sulphates) amount to about -1 to -1.5 W/m^2 (IPCC, 2001; Hansen and Sato, 2001), compared to a positive forcing of +2.5 W/m^2 by the well-mixed greenhouse gases. Absorption of solar radiation by aerosols is primarily due to black carbon (soot) aerosols, and is estimated to exert a forcing of +0.25 to +0.5 W/m^2. The effect of aerosols on cloud properties (indirect radiative forcing) is even more uncertain. IPCC (2001) estimates a net forcing of -1 W/m^2, with an uncertainty of at least a factor of 2. These numbers are estimates at the global scale; regional forcings and their uncertainties can be considerably larger.

Both for the assessment of exposure of the population to PM and for the assessment of climate forcing by anthropogenic aerosols, reducing the uncertainties concerning aerosol or particulate matter abundances is mandatory. At present all EU member states perform air quality measurements to check compliance with the limit values. Ground-based aerosol measurements are relatively precise and available with high temporal resolution, but they are representative for only a limited area, as there can be large spatial concentration gradients particularly in urban areas. Moreover, it is widely recognised that it is very difficult to accurately measure the absolute PM level on a routine basis (CAFE WGPM, 2004). This makes it virtually impossible to achieve a representative overview across Europe based on ground-based measurements only. While chemical transport models are an important tool to improve the understanding of PM concentration distributions, the quality of anthropogenic emission inventories is still seriously hampering models to generate accurate results. Moreover, the contributions from natural sources are hard to quantify, due to limited knowledge of the emission processes. Satellite measurements are less precise than ground based measurements, but they have the advantage that they provide full spatial coverage and are – in principle – consistent for the whole European region. This suggests that satellite measurements may be useful to improve the insight in aerosol distributions in Europe in combination with models and ground based measurements.

In the past few years, many studies have appeared that investigate the usefulness of satellite measurements of AOT for improvement of $PM_{2.5}$ monitoring. Several studies in the U.S. have reported good *temporal* correlations between satellite derived AOT and $PM_{2.5}$ surface concentration measurements in parts of the U.S. (Wang and Christopher, 2003; Hutchison, 2003). In general, promising correlations are found between one-month time-series of AOT

and $PM_{2.5}$ for many stations in the Eastern and Midwest U.S. Other stations, however, particularly in the Western U.S., show hardly any correlation (Engel-Cox et al., 2004). Variations in local meteorological conditions, occurrence of multiple aerosol layers, and variations in aerosol chemical composition likely play an important role in determining the strengths of such correlations. For a location in Europe (the AERONET station at Ispra, Northern Italy), Chu et al. (2003) have shown that time-series of AOT and 24-h average PM_{10} measurements correlate well, for a period of several months in 2001 with stable meteorological conditions. Recently, Van Donkelaar et al. (2006) studied the usefulness of satellite AOT measurements of the Moderate Resolution Imaging Spectroradiometer (MODIS) and the Multi-angle Imaging Spectroradiometer (MISR) for assessment of *spatial* variations of $PM_{2.5}$ in North-America. They concluded that the spatial variation in yearly average $PM_{2.5}$ derived from satellite instruments MODIS and MISR exhibited significant agreement with those from the surface networks in Canada (NAPS) and the U.S. (AQS). They found better agreement using MODIS data than using MISR data. For Europe, the first comparison of spatial and temporal variations in PM and AOT from MODIS was reported in Koelemeijer et al. (2006b), and a more extensive analysis was reported in the PARMA (Monitoring **Par**ticulate **Ma**tter for Climate and Health Effects in Europe) final report (Koelemeijer et al., 2006a). Within that project, Van de Kassteele et al. (2006) applied a statistical approach to map PM_{10} concentrations in Europe using secondary information from MODIS and the LOTOS-EUROS model.

In the PARMA project, MODIS satellite observations of aerosol optical thickness (AOT) were used to improve the mapping of yearly average $PM_{2.5}$ concentrations in Europe in 2003. Similar to the present study, two different approaches were followed to use AOT data for $PM_{2.5}$ mapping: a statistical approach and a data-assimilation approach. In the PARMA project, first the MODIS AOT data were validated against independent AERONET AOT observations. It was found that the spatial correlation of yearly averages MODIS and AERONET AOT data is 0.72 (using the 'fine' fraction of the MODIS AOT, AOT_F). Also the temporal correlation between MODIS and AERONET is generally high. However, the results show that MODIS systematically overestimates AERONET data. The bias could be characterized, however, and corrected for. In the PARMA project, it was concluded that both the statistical mapping and assimilation methods led to a better description of the spatial gradients in the yearly average $PM_{2.5}$ field in Europe as compared to modelled results only. Generally, the spatial features in the $PM_{2.5}$ map based on the statistical mapping approach resembled that of the assimilation approach in the central part of the model domain (North-West Europe).

This report presents the final results of the HIRAM project (**Hi**gh-**R**esolution **A**ir quality **M**onitoring over Europe). The HIRAM project is complementary to and an extension of the project PARMA, which was carried out by MNP and TNO in the period 2004-2006 (Koelemeijer et al., 2006a). Where in the PARMA project satellite data from MODIS were exploited, in the HIRAM project the use of data from AATSR (on board ENVISAT) is investigated. The advantage of AATSR data compared to MODIS is that AATSR observes each atmospheric volume under two different observation angles, one in a forward view, and a few minutes later, in nadir view (i.e., looking straight down to the Earth). This observation strategy allows a better discrimination between surface reflection and reflection by aerosols in the atmosphere, and hence, in principle, a higher accuracy of the retrieved AOT. The AATSR aerosol retrieval algorithm that is currently used by TNO, has been significantly modified with respect to the 'scientific' algorithms that were used in earlier projects, to allow for the automatic processing of large amounts of data. However, it appeared during the course

of the HIRAM project that the current semi-operational algorithm does not provide aerosol information of similar quality as that from the 'scientific' algorithms. Comparison with AERONET stations in Europe shows that in nearly 40% of the cases the time correlation is less than 0.5. Furthermore, the spatial distributions in the AATSR AOT data for 2003 are different from those observed by MODIS in 2003 and by ATSR-2 in August 1997 (Roblez-Gonzales et al., 2000; Roblez-Gonzales et al., 2003), and are not in agreement with aerosol distributions expected from chemical transport model calculations. In particular, the current AATSR algorithm performance appears to provide unrealistic results over northern Europe (Ireland, UK, Scandinavia and Finland). It is likely that the reduced performance of AATSR (compared to MODIS or ATSR-2) is at least partly due to the performance of the automatic cloud detection procedures. Therefore, a major part of this study has been devoted to the *validation* of AATSR data as provided using the current semi-operational algorithm, through comparison with AERONET ground based measurements of AOT. As part of the validation, a method was developed to estimate the percentage of cloud contaminated satellite AOT data. Also, criteria were developed by which part of the erroneous data could be identified and removed. These 'screened' AATSR data could however no longer be used to study AOT at a high spatial resolution, because too few data were left after this screening to allow a meaningful analysis at high spatial resolution. The *analysis* part of this study has therefore focussed on analysing $PM_{2.5}$ variations over Europe at 10x10 km^2 resolution. The results have been compared to those obtained in the PARMA project. Also, an analysis is made of trends in radiative forcing by sulphate and nitrate aerosols.

The report is structured as follows. The primary data sources for the analysis of $PM_{2.5}$, AATSR and AirBase, are described in chapter 2. The AATSR AOT measurements are presented in chapter 3, and an initial assessment of AATSR data is made there by comparing to ATSR-2 and MODIS data. In chapter 4, a quantitative validation is performed using independent AOT observations from the ground based AERONET network, and cloud contamination issues are discussed in detail. In that chapter, also a methodology is described how AATSR data are treated in the analysis part of the project, and a quantitative comparison is made with the MODIS data as used in the PARMA project. In chapters 5 and 6, $PM_{2.5}$ analyses are presented using the statistical mapping and assimilation approaches, respectively. In chapter 7, an analysis is made of trends in radiative forcing by sulphate and nitrate aerosols. Conclusions are presented in chapter 8.

2. Data sources

Measurements of aerosol optical thickness were obtained from the AATSR instrument on ENVISAT. The AATSR instrument and retrieval method have been described in section 2.1. Daily and hourly particulate matter measurements were extracted from the AirBase database, and are described in section 2.2.

2.1 Aerosol optical thickness from AATSR

2.1.1 The AATSR instrument

The Advanced Along-Track Scanning Radiometer (AATSR) instrument onboard the European ENVISAT satellite revolves the Earth at an altitude of approximately 800 km in a sun-synchronous polar orbit. The AATSR is almost identical to the ATSR-2 instrument, and has seven wavelength bands in the visible and infrared parts of the spectrum (measurement wavelengths are at 0.55, 0.67, 0.87, 1.6, 3.7, 11 and 12 μm; see Koelemeijer et al., 1998). The instrument has a conical scanning mechanism providing two views of the same location with a resolution of 1x1 km^2 at nadir view. The radiometer views the surface along the direction of the orbit track at an incidence angle of 49° as it flies toward the scene and some 150 seconds later it records a second observation of the scene at an angle close to the nadir view. The swath width of 512 km results in an overpass over a given location in Europe every three days. An AOT retrieval at each location can only be made in cloud-free conditions, however.

2.1.2 Retrieval procedure

The semi-operational AATSR algorithm that is used for HIRAM is based on the scientific ATSR-2 algorithms developed by Veefkind et al. (1998a, 1998b, 1999, 2000) and Robles González et al. (2000). The dual view is used over land and a single view is used over water. The aerosol properties retrieved with these algorithms are the aerosol optical thickness (AOT) at the available wavelengths (0.55, 0.67, 0.87 and 1.6 μm) and the Ångström coefficient α that provides the AOT wavelength dependence which contains information on the shape of the aerosol size distribution. Over land the AATSR dual view algorithm uses both the forward and the nadir view to eliminate surface reflections (see Flowerdew and Haigh, 1995) from the total reflected solar light measured at the top of the atmosphere. This is necessary because the land surface reflections are variable and often of similar magnitude as the aerosol signal. If the land reflectance is not properly accounted for, this may lead to large errors in the retrieved aerosol parameters. Retrievals are available on the scale of the pixel size of 1x1 km^2 (level 2) and averaged over larger scales (level 3) for European maps. AATSR satellite measurements of the radiation at the top of the atmosphere are input for the semi-operational AATSR aerosol retrieval algorithm. The AATSR swath of 512 km allows for an overpass over each geolocation every three days, between 10 and 11 A.M. The retrieval method follows the schematic in Figure 2.1.

The aerosol model used in this work is an external mixture of anthropogenic aerosol (sulphate/nitrate water soluble) and sea salt. The effective radius of the anthropogenic aerosol is 0.05 μm. The optical properties are based on the anthropogenic water soluble aerosol with effective radius r_{eff} = 0.03 μm as defined in Volz (1972). The sea salt aerosol has an effective radius of 1 μm with optical properties as defined in Shettle and Fenn (1979). A Mie scattering code and the Radiative Transfer Model DAK (Stammes, 2001) are used for the generation of

Look-up tables (LUTs). Cloud-free pixels are essential for a proper retrieval of aerosol properties; hence an automatic cloud detection procedure is used consisting of three tests for cloud detection. These tests are based on cloud detection routines initially developed for off-line (manually supervised) application by Koelemeijer et al. (2001). The method was adapted for semi-automatic application by Robles González et al.(2003) to allow processing of larger datasets in reasonable time. After cloud detection, radiative transfer calculations are performed to correct the measured satellite signal for absorption by ozone, for contributions by the surface and for molecular (Rayleigh) scattering. Finally, the corrected TOA (Top of the Atmosphere) reflectance at the satellite sensor is compared with the modelled reflectances in iterative steps in order to select the right aerosol mixture. This procedure is based on a look-up table approach. Measured and modelled reflectances are matched using an error minimization procedure to determine the most likely aerosol mixture and the AOT for the available AATSR wavelengths (Robles González et al., 2000; 2003).

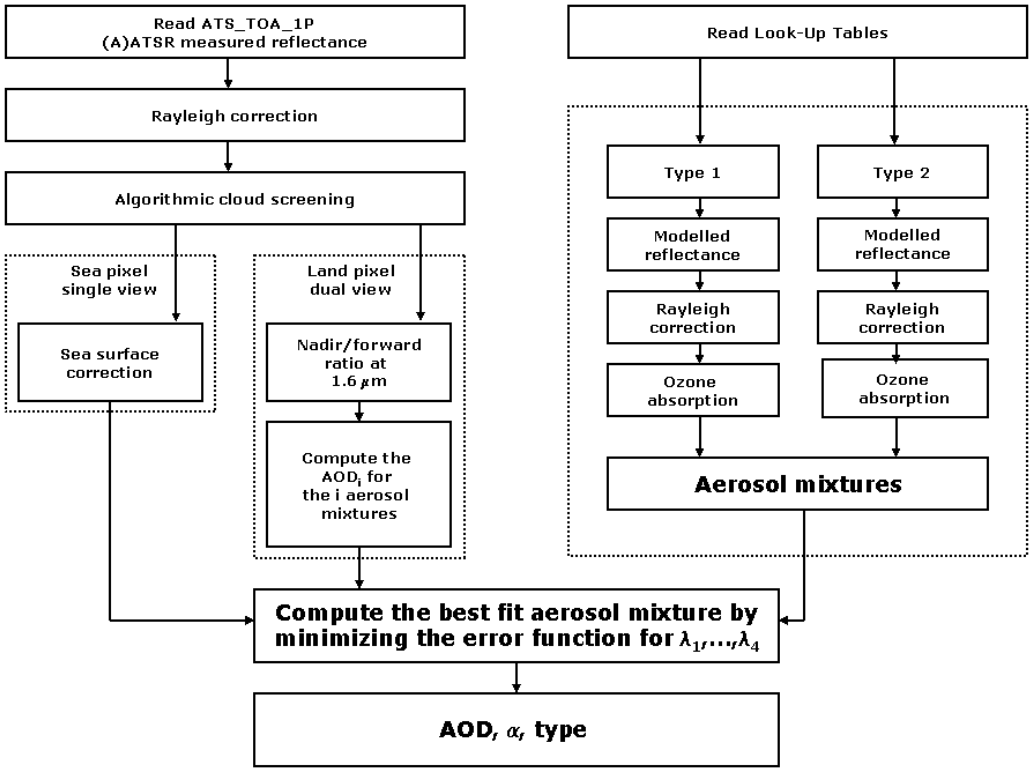

Figure 2.1 Schematic overview of the semi-operational retrieval algorithm.

Daily AOT maps over Europe are produced for the 1x1 km^2 sensor resolution. The final AOT maps for the European scale are given as a product with a resolution of 10x10 km^2 (roughly 0.1^o x 0.1^o over Europe) by means of an automatic post-processing step, where the AOT values for the individual AATSR pixels in each 10x10 km^2 area are averaged.

2.2 Particulate matter concentrations from AirBase

Since the adoption of the EU air quality directives (EU, 1996; 1999), mass concentration measurements in Europe are performed operationally for particles smaller than 10 micron in diameter (PM_{10}). In the past few years, also more and more measurement sites are emerging for particles smaller than 2.5 micron in diameter ($PM_{2.5}$), as a new air quality standard for $PM_{2.5}$ will complement the current PM_{10} standard.

These PM data are submitted to the AirBase data of the European Topic Center on Air and Climate Change (ETC-ACC) of the European Environment Agency (EEA). This database consists of hourly or daily averaged values of PM, and meta-data, such as the latitude and longitude coordinates of the station, its altitude, and information on its surroundings (urban background, (sub)urban background, street, industrial), measurement technique, et cetera.

The EU reference method to measure PM_{10} concentrations is described in CEN standard EN 12341, adopted by CEN in November 1998 (EN 12341, 1998). The mass collected on the filter is determined gravimetrically by means of a microbalance under well-defined environmental conditions. This is the reference method under the First Daughter Directive and gives, by definition, the 'correct' PM_{10} results. However this method is not suitable for operational application. For operational measurements, often the beta-absorption method and tapered element oscillating microbalance (TEOM) are used. In the beta-absorption method, the amount of particles on the filter is determined by measuring the attenuation of a beam of beta-radiation (electrons) which are send through the filter. The attenuation is proportional to the mass of the aerosols on the filter. The TEOM makes use of the change in eigen-frequency of a tapered glass element that is connected to the filter. The change in eigen-frequency is determined by the mass of particles attached to the filter. Operational measurements of *absolute* levels of PM have considerable uncertainty. A major reason for this is volatilization of aerosols because of heating the air sample in the measurement process. This heating is necessary to avoid humification of the filter. The amount to which volatilization occurs depends on the environmental conditions and composition of the particles. Often the results from beta-absorption instruments as well as the TEOM underestimate the concentration due to these problems (e.g. Hitzenberger et al., 2004; Charron et al., 2004). Therefore, if beta-absorption or TEOM is used to determine PM, measurement results have to be corrected by a correction factor to produce results equivalent to the reference method. These correction factors can vary substantially in space and even seasonally (CAFE-WGPM, 2004). Differences between correction factors and the application itself hamper integration on a European scale of all PM_{10} data. An overview of correction factors used for data in the AirBase database is given in Buijsman and De Leeuw (2004).

No European Reference Method for the measurement of the $PM_{2.5}$ fraction has been established up to now. Such a standard is currently being developed by CEN (CEN TC 264/Working Group 15) under a mandate of the European Commission. As for PM_{10}, the method is based on the gravimetric determination of the $PM_{2.5}$ fraction of particles in the air, sampled at ambient conditions. For operational applications, often the beta-absorption and TEOM methods are used, but no overview exists of correction factors and their application.

Most PM measurement stations are representative for background conditions in rural, sub-urban and urban areas. In this study we have used rural background stations only, because these are representative for areas that are comparable to the size of an AOT measurement. In 2003, 28 European countries submitted their PM_{10} data and 11 countries their $PM_{2.5}$ data to AirBase. Most stations only deliver daily averaged PM concentrations to AirBase. From the 88 $PM_{2.5}$ stations that delivered daily average data, 23 stations also delivered hourly data. The meta-information in AirBase includes a description of the surroundings (rural, suburban of urban), the type of station (traffic, background, or other), the measurement method used, the altitude et cetera. A number of elementary quality checks have been done on the AirBase data, such as removing data from stations with clearly erroneous latitude/longitude coordinates.

3. Initial assessment of AATSR AOT data

In this chapter, AATSR AOT maps are presented for 2003, and a qualitative comparison is made between AOT maps derived from ATSR-2 (August 1997), AATSR (2003), and MODIS (2003).

The image of ATSR-2 derived monthly average aerosol optical thickness for August 1997 is shown in Figure 3.1 (top left) (Robles González et al., 2000). Large variations in mean AOT are observed across Europe. For example, mean AOT values of 0.5-0.6 occur over certain areas over Germany, Belgium, the South of the Netherlands and Northern Italy. In contrast, AOT values of 0.1 to 0.2 were observed over Scandinavia, Central Spain, Southern France and Russia. The high AOT values are often associated with strongly industrialized areas, with large emissions of both primary PM emissions and aerosol precursor gases (SO_2 and NO_x). Sudden increases of a factor of 3 or more over relatively short distances may be accompanied by a gradual decrease over hundreds of km, presumably down wind from the source. An example is the variation of AOT over Western Germany and Belgium. Strong gradients are also observed in northern Italy. Aerosols produced in the heavily industrialized areas around Milan and Turin are trapped in the Po Valley. Because the Alps in the North and the Apennines in the South form natural barriers, aerosols can only be vented through the Po Valley to the Adriatic Sea (Robles González et al., 2000).

The MODIS yearly average AOT_F (fine fraction AOT) for 2003 was used in the PARMA study and is depicted in Figure 3.1 (top right). The MODIS map of 2003 shows, to some extent, similar spatial structures as that derived from the ATSR-2 map of August 1997. The Po Valley and Benelux area also show up in the MODIS map, as well as high values in Central-Europe and the Balkan countries, albeit that over Northern Germany and Poland, the MODIS AOT is substantially higher than that of ATSR-2 in August 1997. Part of this difference between 2003 and August 1997 can be ascribed to differences in the meteorological conditions, particularly over Poland (see sections 6.3 and 6.4).

The initially retrieved yearly average map of AOT for 2003 derived from AATSR (i.e., without additional cloud/snow screening) is shown in Figure 3.1 (bottom, left). It is clear that the spatial structures are very different from the AOT distribution derived from ATSR-2 for August 1997, and from the MODIS map of 2003. The annual average AOT values from AATSR in 2003 show unrealistically high values in Northern Europe, particularly in Ireland, UK, Scandinavia and Finland, and over mountain regions (Alps, Pyrenees). Furthermore, it is apparent that large cities cannot be distinguished clearly in the 2003 data, in contrast to the ATSR-2 data of August 1997.

It is likely that the difference between the ATSR-2 image of August 1997 and the AATSR image for 2003 is caused by a difference in cloud detection algorithm. In case of August 1997, the semi-automatic cloud detection was checked visually, whereas a fully automatic procedure was used for 2003. Visual inspection of individual images was not possible for this large dataset. As a result however, it is likely that relatively many cloud or snow-contaminated AATSR pixels have erroneously been classified as cloud-free in the AATSR data of 2003, which leads then to unrealistically high values for the retrieved AOT. This issue is further investigated in chapter 4.

Due to these problems the AATSR results per se could not be used for mapping PM distributions. A severe data selection has been applied in an attempt to partly resolve this problem (see section 4.3). This leads to an large reduction of the number of useable data points (Figure 3.1, bottom right), but what is left appears more realistic than the initial retrieval. Obviously, such data selection could be avoided if the AATSR algorithm would be improved, which is imperative for the future use of this algorithm.

In conclusion, the AATSR data for 2003 show large differences compared to MODIS data for 2003 and ATSR-2 data of August 1997. Given these differences, we have put emphasis on the validation of the AATSR and MODIS products in this study.

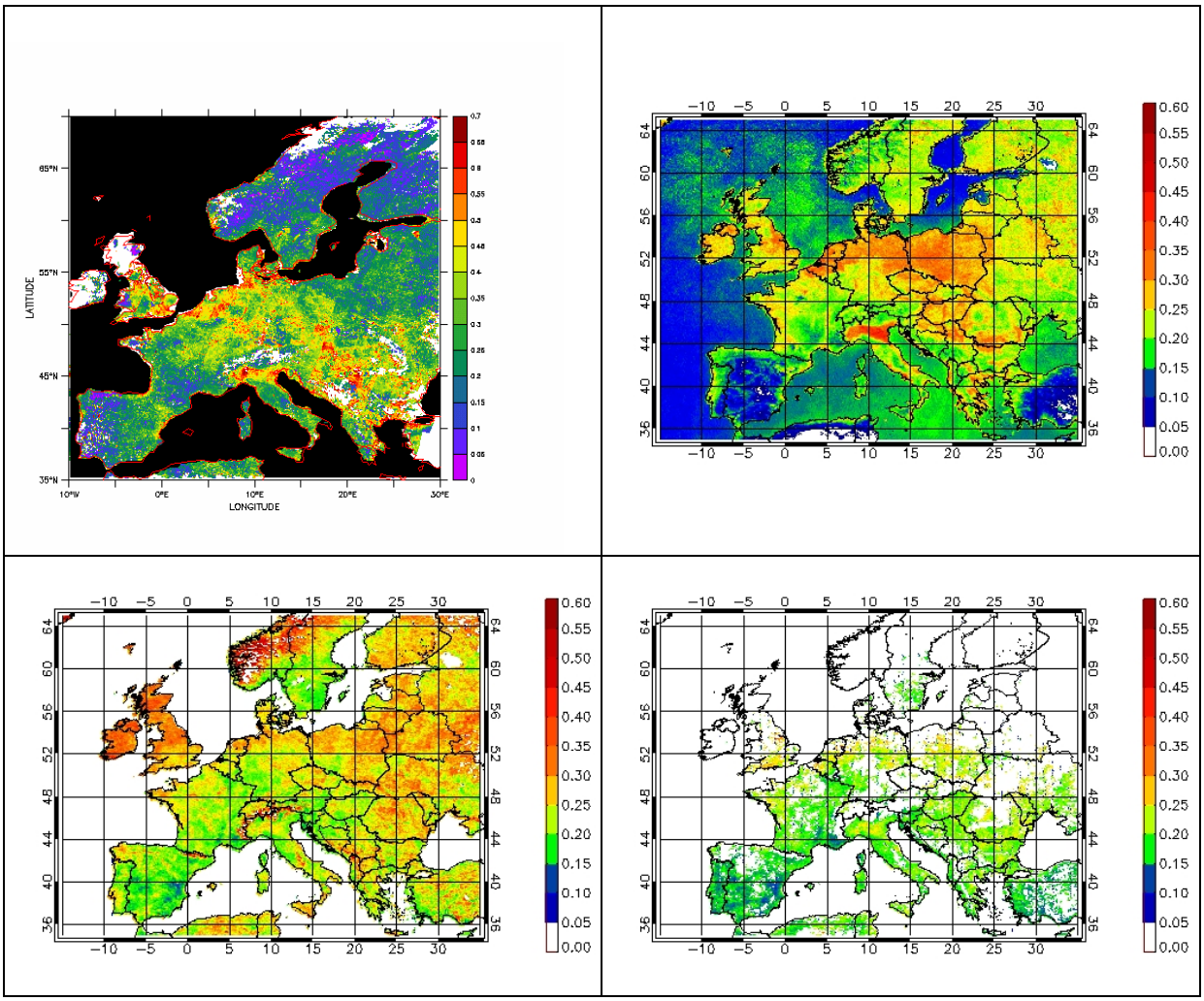

Figure 3.1 Aerosol optical thickness over Europe derived from ATSR-2 data (top left, average August 1997), MODIS (top right, average 2003) and AATSR (bottom left, initial average 2003) and AATSR (bottom right, screened average 2003). White area: no data available.

4. Validation of AATSR

In section 4.1, AATSR validation is performed by comparing the AATSR retrieved AOT values with ground-based measurements of AOT from the AERONET network. This validation is – by definition – limited to nearly cloud-free conditions, as AERONET data of AOT are only available under nearly cloud-free conditions. The extent to which AATSR (and MODIS) data are affected by cloud contamination is therefore estimated in section 4.2. The consequences of the validation results for the analysis part of this study are described in section 4.3. In that section additional cloud-detection checks are suggested (applicable to monthly average data only). The resulting monthly and yearly average AOT map (i.e., after application of these additional checks) are referred to as 'screened' AATSR data. A detailed comparison of these 'screened' AATSR data with MODIS data is presented in section 4.4.

4.1 Validation of AATSR using AERONET

AERONET is a ground-based global network consisting of many sun photometers that measure the AOT in the atmospheric column from ground to sun, with an accuracy between ±0.01 and ±0.015 (Eck et al., 1999). This accuracy is considerably higher than the retrieval accuracy of current satellite instruments like AATSR and MODIS, and hence is suited for validation. In the past, limited validation of ATSR-2 retrievals over Europe using AERONET has indicated agreement of AOT values of ATSR-2 and AERONET within ±0.06 over land and ±0.04 over sea (Robles González et al., 2003).

Here an extensive validation of AATSR data has been performed for Europe for 2003. The validation results for AATSR have been compared with validation results of MODIS, to allow comparison with the PARMA study (Koelemeijer et al., 2006a). The validation statistics are shown in Table 4.1. Only stations are shown with more than ten days with both AATSR and AERONET data. AERONET AOT data were acquired between 9:00 and 11:00 hours, i.e., close to the time of the AATSR overpasses (10:00), and between 11:00 and 13:00 hours, i.e., close to the time of the MODIS overpasses (10:30 and 13:30). The comparison results of MODIS and AERONET are slightly different compared to the PARMA study, as the number of stations is more limited here.

The first observation is that the yearly average AOT retrieved from AATSR has only a small bias compared with AERONET. Averaged over all stations the bias is zero on average. MODIS systematically overestimates the AOT (bias averaged over all stations is +0.04 using the AOT_F). In the PARMA study, it was found however, that the bias in MODIS AOT and AOT_F showed a distinct seasonal variation, and could therefore be partly characterized and corrected for in a straightforward manner. The standard deviation of the difference between AATSR and AERONET is ±0.13, based on all 760 pairs AERONET-AATSR in the 2003 dataset. In case of MODIS AOT_F, and after correcting for the time-dependent bias according to the PARMA study, the standard deviation is ±0.11, based on 3400 pairs of MODIS-AERONET in the 2003 dataset, and after correcting for the time-dependent bias in the AOT_F. Hence, the standard deviation of the difference with AERONET is slightly higher for AATSR compared to MODIS. The 1-sigma RMS-error of MODIS of ±0.11 is consistent with that quoted in the literature, which is ±0.05±0.2*AOT.

However, the *time* correlations of AATSR with AERONET are less than 0.50 for nearly 40% of the stations. A similar comparison shows a better performance for MODIS (15% has a time correlation smaller than 0.50). The time correlation averaged over all stations is 0.53 (0.59 median), while it was 0.65 (0.73 median) using MODIS data. It is apparent that stations with a low time-correlation often correspond to stations where AATSR has a much higher yearly average AOT than AERONET (Belarus, Estonia, Russia, Sweden). This suggests that there is residual cloud contamination in the satellite data leading to too high AOT values and low correlation coefficients. It is also apparent these stations are predominantly located in Northern and Eastern Europe. The *spatial* correlation between yearly average AOT values from AATSR and AERONET is very low (0.36) whereas for MODIS it was 0.72 (using the AOT_F).

The number of collocated pairs of AERONET and AATSR data is about five to six times lower than the number of collocated pairs using MODIS data. This is because MODIS has a much higher temporal coverage (twice daily) compared to AATSR (once every three days for Europe).

Table 4.1 Statistics of AOT observations of AERONET and AATSR in Europe in 2003. For comparison, MODIS AOT_F observations are shown as well.

		Number of pairs		AERONET	MODIS	AERONET	AATSR	Time correlation	
country	station	MODIS	AATSR	(12 h)		(10 h)		MODIS	AATSR
Belarus	Minsk	56	18	0.21	0.24	0.13	0.25	0.85	-0.20
Belgium	Oostende	98	14	0.27	0.39	0.24	0.25	0.82	0.66
Estonia	Toravere	56	14	0.14	0.18	0.13	0.16	0.33	0.19
France	Avignon	230	49	0.19	0.28	0.19	0.15	0.79	0.44
France	Dunkerque	51	13	0.19	0.24	0.11	0.23	0.75	0.40
France	Fontainebleau	97	16	0.20	0.22	0.20	0.18	0.79	0.59
France	Lille	92	16	0.22	0.31	0.17	0.18	0.88	0.84
France	Palaiseau	103	19	0.25	0.28	0.26	0.19	0.74	0.68
France	Toulouse	151	26	0.18	0.23	0.18	0.16	0.63	0.53
Germany	Hamburg	109	25	0.18	0.26	0.17	0.19	0.78	0.46
Germany	IFT-Leipzig	66	17	0.22	0.37	0.26	0.23	0.78	0.90
Germany	Munich	44	11	0.18	0.27	0.21	0.19	0.62	0.74
Greece	Forth Crete	154	40	0.20	0.15	0.21	0.17	0.52	0.63
Italy	IMC Oristano	175	30	0.20	0.22	0.25	0.15	0.47	0.68
Italy	ISDGM CNR	187	48	0.26	0.41	0.21	0.23	0.85	0.89
Italy	Ispra	160	49	0.31	0.28	0.21	0.19	0.65	0.76
Italy	Lecce University	173	36	0.21	0.24	0.24	0.19	0.61	0.73
Italy	Rome Tor Vergata	208	49	0.23	0.24	0.22	0.16	0.71	0.24
Italy	Venise	201	51	0.21	0.23	0.20	0.24	0.72	0.77
Moldova	Moldova	16	11	0.22	0.15	0.21	0.22	0.74	0.39
Portugal	Evora	66	24	0.16	0.08	0.15	0.15	0.53	0.65
Russia	Moscow	59	24	0.21	0.31	0.16	0.27	0.16	0.20
Spain	El Arenosillo	184	46	0.16	0.22	0.14	0.16	0.75	0.40
Spain	Palencia	56	20	0.14	0.08	0.14	0.15	0.07	0.55
Sweden	Gotland	87	25	0.13	0.22	0.13	0.17	0.77	0.07
Turkey	IMS METU	168	33	0.23	0.28	0.24	0.18	0.70	0.58
average		**117**	**28**	**0.20**	**0.24**	**0.19**	**0.19**	**0.65**	**0.53**
median		**101**	**25**	**0.20**	**0.24**	**0.20**	**0.18**	**0.73**	**0.59**

For a few stations, time series have been investigated in more detail. For Avignon, the correlation over the entire year 2003 is 0.44. Figure 4.1 (top) shows the time series of both AERONET and AATSR at this station. The agreement between both measurement methods is reasonably good over the summer period, however at the end of the year some AATSR measurements show larger deviations from the AERONET measurements, and are higher than the AERONET measurements. Indeed the correlation over the April-September period is much higher, 0.74 than over the entire year. The station ISDGM-CNR has a high correlation of 0.89 and does not show these large differences between AATSR and AERONET (Figure 4.1, bottom). After investigation, the deviating points visible in the AATSR time series of Avignon correspond to average AOT values at 10x10 km^2 resolution where only a few measurements were available. This indicates that the other AATSR 1x1 km^2 pixels in this 10x10 km^2 area are identified as cloudy. It is possible however that the 1x1 km^2 pixels identified as being clear are in reality also contaminated by clouds.

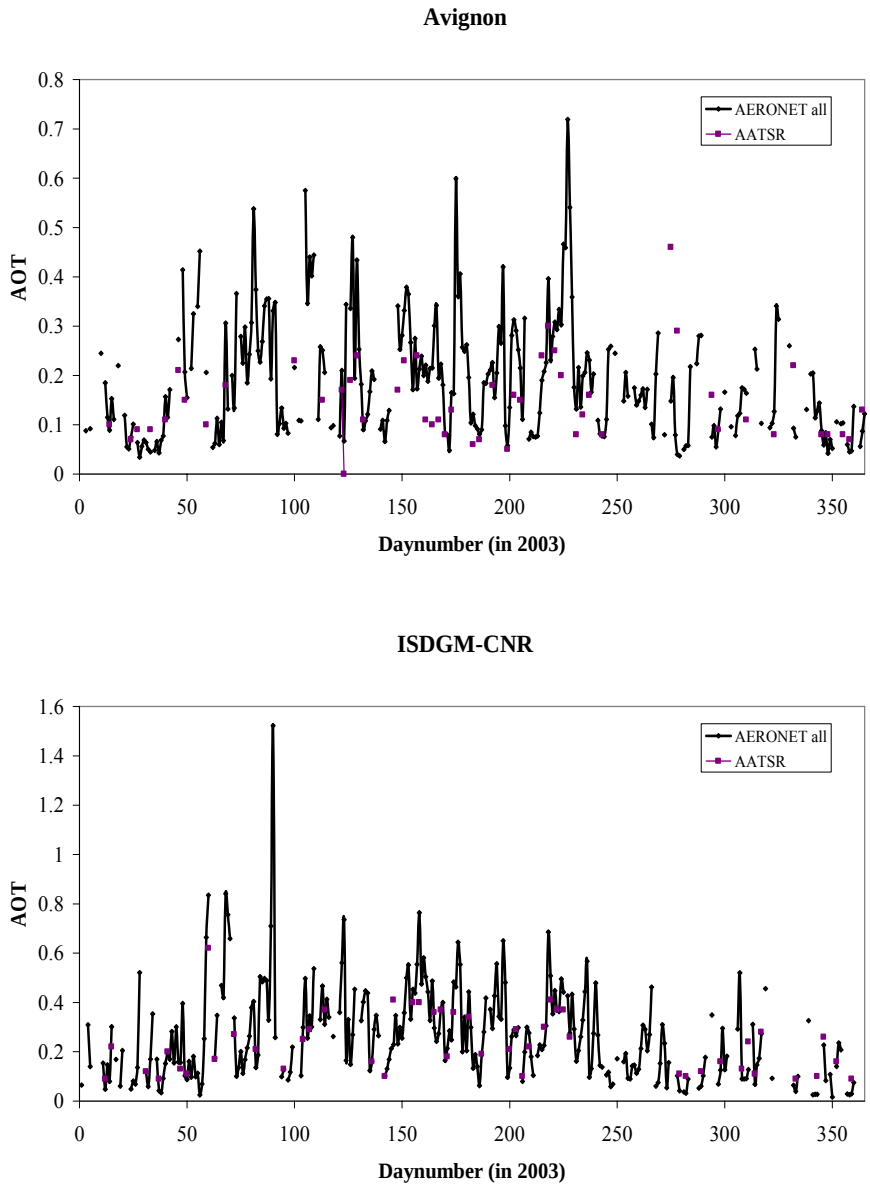

Figure 4.1 Temporal variation of AERONET AOT and AATSR AOT Avignon (France, top) and at ISDGM-CNR (Italy, bottom).

4.2 Cloud contamination issues

The validation with AERONET is by definition biased to clear-sky situations, as only AERONET AOT data are available under (nearly) cloud-free conditions, such that an AOT measurement can be made by AERONET. Hence, in the validation of AATSR, data with erroneous cloud detection are under-represented in the validation dataset, as these will occur more often under (partly) cloudy situations. Therefore we have also assessed the number of AATSR (and MODIS) retrievals over AERONET stations, which do have satellite AOT value but miss a AERONET retrieval. In this manner, we determine the number of observations that could erroneously be identified as cloud-free. The results of this analysis are shown in Tables 4.2 and 4.3.

Table 4.2 'Score card' for MODIS and AATSR cloud detection.

		MODIS observation		AATSR observation	
		yes	**no**	**yes**	**no**
AERONET observation	**yes**	161	11	33	121
	no	80		32	

Fist we discuss the results for MODIS. Table 4.2 shows that, *averaged over all AERONET stations*, 161 cases occurred where both MODIS and AERONET have AOT measurements, indicating clear-sky conditions. However, there are 80 cases where MODIS provides an AOT retrieval where AERONET does not have a measurement. This might indicate that the MODIS cloud detection is not strict enough in these cases. So, on average, 33% of the MODIS data might suffer from cloud contamination to some extent. We refer to this percentage as the percentage of potentially cloud-contaminated data (PCCD). Note that there are only a few cases (11) in which AERONET does have a measurement and MODIS does not have a measurement.

Table 4.3 Percentage of Potentially Cloud Contaminated Data (PCCD) of MODIS and AATSR at AERONET stations that were operational throughout 2003.

country	**station**	Latitude	Longitude	**MODIS**	**AATSR**
Belarus	Minsk	53.00	27.50	48%	67%
Belgium	Oostende	51.23	2.93	44%	77%
France	Avignon	43.93	4.88	16%	30%
France	Fontainebleau	48.41	2.68	45%	74%
France	Lille	50.61	3.14	47%	74%
France	Palaiseau	48.70	2.21	38%	66%
France	Toulouse	43.57	1.37	30%	60%
Germany	Hamburg	53.57	9.97	39%	62%
Greece	Forth Crete	35.33	25.28	22%	38%
Italy	IMC Oristano	39.91	8.50	32%	58%
Italy	ISDGM CNR	45.44	12.33	14%	26%
Italy	Ispra	45.80	8.63	28%	32%
Italy	Lecce University	40.33	18.10	31%	45%
Italy	Rome Tor Vergata	41.84	12.65	23%	36%
Italy	Venise	45.31	12.51	14%	12%
Portugal	Evora	38.57	-7.91	60%	64%
Spain	El Arenosillo	37.11	-6.73	29%	32%
Turkey	IMS-METU	36.57	34.26	42%	49%
	mean all stations			**33%**	**50%**

Application of this method to AATSR shows that on average 50% of the AATSR data can be contaminated by clouds. It is also apparent that many cases exist (121) where AERONET does have a measurement and AATSR does not have a measurement. This can be explained to a large extent by the fact that AATSR does not have a daily coverage for Europe, but only once every three days. Table 4.3 shows the PCCDs for the individual stations. Only stations are listed that provided measurements throughout the whole of 2003. Note that most of the stations are located in Southern Europe, and that the PCCD values in Northern Europe may be higher. The PCCD values range between 10% and nearly 80%. For stations in Southern Europe, MODIS and AATSR PCCD values are closer to each other than for stations at higher latitudes. With increasing latitude, both AASTR and MODIS PCCD values increase, but the PCCD values of AATSR more strongly increase with latitude than those of MODIS. This indicates relatively more cloud contaminated pixels at higher latitudes in both AATSR and MODIS, but more strongly so for AATSR.

It is noted that the PCCD analysis above might be too pessimistic because of two reasons:
(1) In the analysis it is assumed that the AEONET stations were fully operational throughout the year. We have therefore selected those AERONET stations that had data available both at the beginning and at the end of the year. Furthermore we have only used AERONET stations that had more than 100 days with observations in 2003; these coincided with the stations that had data throughout 2003. Nevertheless, it might happen that AERONET has no data because of technical reasons, such as power failure, and not because of cloudy conditions.
(2) It is also possible that AERONET has no data, while the satellite has valid data, because of partly cloudy conditions. In these conditions it may happen that clouds occur in the line of sight between the sun and the AEONET station, whereas directly above the AERONET station it can be cloud-free. This situation can also occur because of time differences between the satellite and AEORNET observation, as in the meantime the cloud situation may have changed. This also means that for MODIS the PCCD analysis may be slightly more pessimistic than for AATSR, as the time-difference between MODIS and AERONET is generally larger (typically 1:30h) than for AATSR (typically 1:00h). Despite these limitations, it is felt that these two aspects are of relatively minor importance.

4.3 The use of AATSR data in the analysis part of the study

As sketched in chapter 3 and the first sections of chapter 4, for several reasons, the AATSR retrieved AOT, using the current version of the algorithm, have a number of shortcomings resulting in problems regarding their use for air quality mapping:
1) The large scale distribution of AOT from AATSR in 2003 appears unrealistic, in particular the high values in Ireland, the UK, Scandinavia and Finland. We cannot recognize large point sources, or source areas such as major cities and even larger scale hot-spot regions can barely be detected.
2) Validation with AERONET has shown that AATSR has a much lower correlation in time and space as compared to MODIS.
3) It was shown that on average about 50% of the AATSR data in 2003 is potentially contaminated by clouds (or snow); the contamination increases towards higher latitudes.
4) The number of AATSR observations is limited because of the small swath width. It turns out that in practice about 65 observations are available per year for a given location. This means about one observation every six days, and only half of these are not potentially

contaminated by clouds or snow. In contrast, MODIS has about 240 observations per year for a given location, of which one-thirds is potentially contaminated by clouds.

The statistical mapping approach makes use of yearly average data. The advantage of this approach is that this method can still work reasonably well with only limited amount of data, although it should be sufficient to calculate a yearly average. Hence, the procedure may profit from a rigorous data reduction. Therefore, to limit the influence of cloud and snow contamination in the AATSR retrieved values are similar to the monthly average was based on at least 150 individual retrievals in a 0.1x0.1 degree grid, and for which the standard deviation of the individual AOT retrievals was 0.25 or smaller. The latter criterion assumes that a large standard deviation indicates the possibility of outliers due to undetected clouds or snow coverage. These data are no longer considered. This leads to an rigorous reduction of the number of data points (see Figure 3.1, bottom right), but what is still left appears more realistic than the initial retrieval. These 'screened' data are used in the statistical approach to investigate the mapping of $PM_{2.5}$ in chapter 5.

Unfortunately, for the assimilation method, instantaneous data are needed. Hence, the performance of the system is dependent on the number and quality of the individual data. A data reduction approach based on monthly statistics does not work, as the influence of an assimilated swath is only present for about two days. The maximum possible coverage of AATSR is already suboptimal for an assimilation study. A rigorous data reduction would result in too few data points for a sensible application of the assimilation system. In an attempt to reduce the number of cloud-contaminated AATSR pixels in the assimilation, we have used the cloud-detection results from AERONET observations whereas MODIS instead. An example of this method is shown in Figure 4.2. The biased high AOT values in Northern Scandinavia (top, left) are filtered out of the AATSR data when the cloud-detection of MODIS (top, right) is applied to the AATSR-data (bottom, left). This method is applied in the assimilation approach in chapter 6.

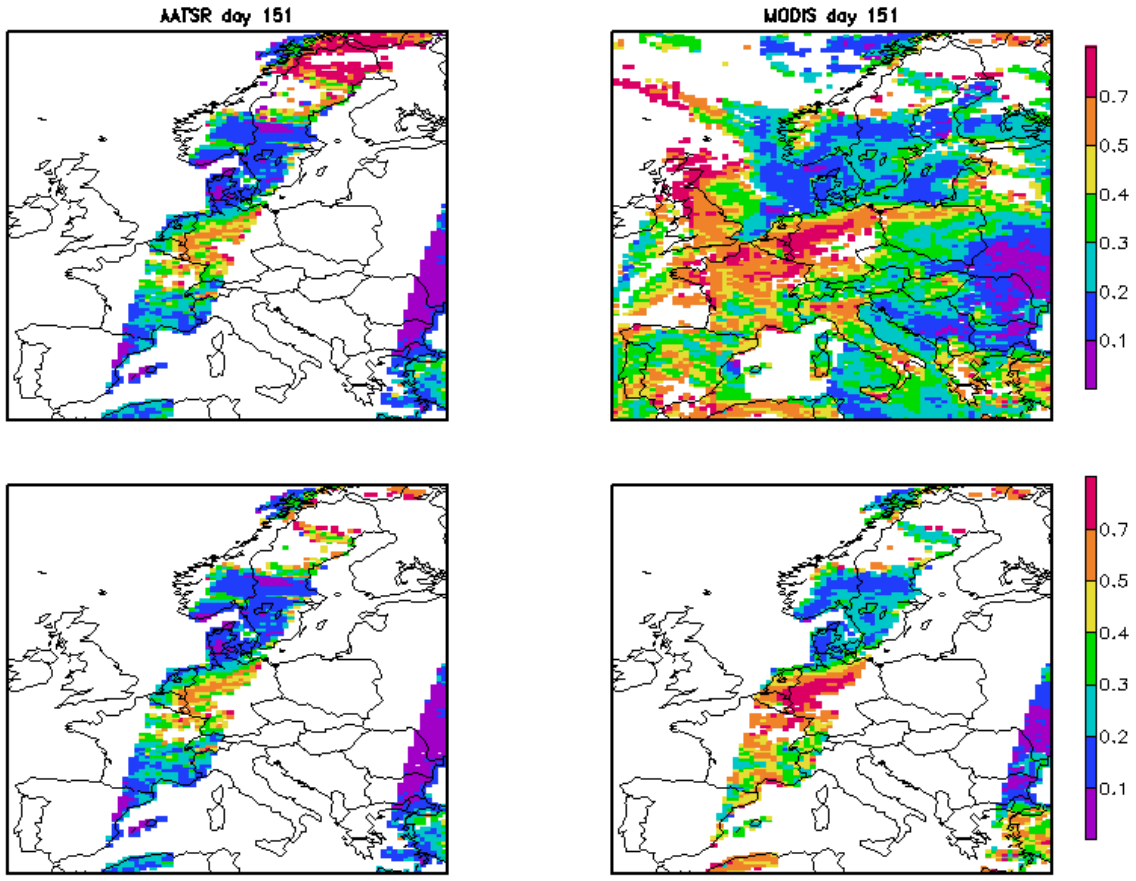

Figure 4.2 AOT values for AATSR and MODIS for 31 May 2003. The lower two plots only comprise collocated measurements.

4.4 Comparison of 'screened' AATSR data with MODIS

Figure 4.3 shows the resulting AOT map for the year 2003 together with the number of months on which the local yearly average AOT values are based, as obtained after additional screening for cloud contamination. These data are used in Chapter 5 for mapping $PM_{2.5}$. From the monthly mean AOT values a yearly average was calculated if at least six months of data were available. It can be observed that over large parts of Europe the temporal coverage is insufficient to determine the yearly average. This is the case over Scandinavia and Finland (with the exception of parts in southern Sweden), over Ireland and parts of the United Kingdom, over large parts of Central and Eastern Europe, as well as over the Alps. Over regions with sufficient data coverage, a clear north-south gradient can be observed with the highest yearly average AOT values on the order of 0.2-0.3 over the Southern United Kingdom, the northwestern part of Belgium, the Netherlands, Germany, and Poland and lower values on the order of 0.1-0.2 over the Mediterranean countries of Southern Europe. Increased AOT values are also observed in Northern Italy over the Po valley. These results are now at least in qualitative agreement with the patterns observed by MODIS, and what might be expected from air quality modelling.

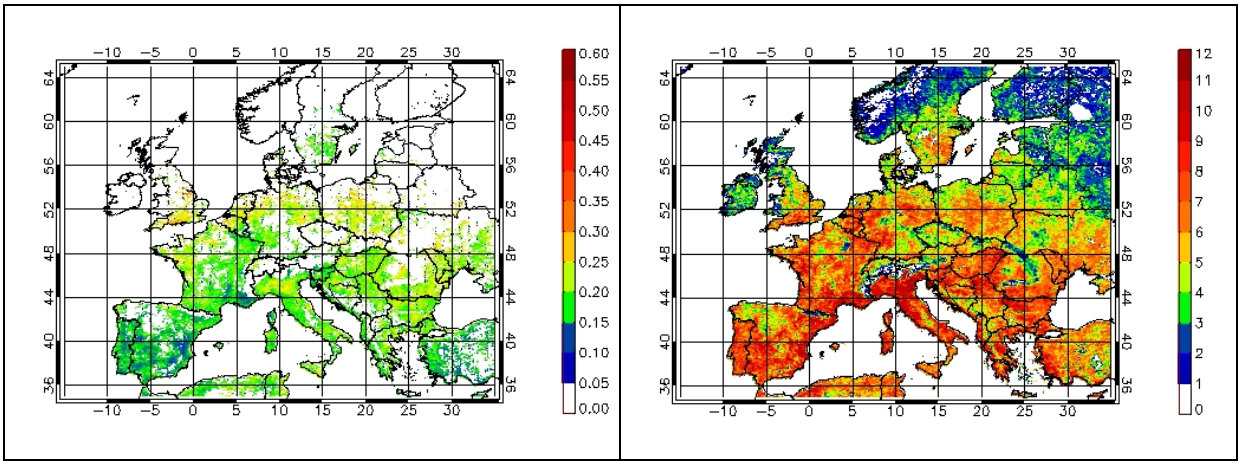

Figure 4.3 Yearly average map of the aerosol optical thickness over Europe derived from AATSR data for 2003 (left), together with the number of months on which yearly average values are based (right). If the number of months for averaging smaller than six, no yearly average is calculated.

The AATSR data have been compared quantitatively with the AOT_F (the fine-fraction of the AOT) from MODIS. We have chosen the AOT_F from MODIS, because that quantity was used to map $PM_{2.5}$ in the PARMA study. It was found that the spatial correlation coefficient between the yearly AOT retrieved from AATSR and the yearly average AOT_F from MODIS is 0.58. This indicates that these different satellite instruments show substantial spatial differences in yearly average aerosol optical thickness over Europe. To investigate the spatial structure of the difference between AATSR and MODIS, the ratio of the yearly average AOT from AATSR and the yearly average AOT_F from MODIS is shown in Figure 4.4. For the interpretation of these maps it should be realized that ratios lower than unity indicate that AATSR underestimates the AOT compared to MODIS. Note that this does not mean that AATSR overestimates the AOT compared to AERONET, however, as MODIS overestimates the AOT compared to AERONET. Ratios higher than unity indicate either that AATSR overestimates the AOT_F compared to MODIS or that a significant fraction of the AOT is related to particles in the coarse mode. The latter reason can be underlying the high AATSR AOT/MODIS AOT_F ratios over large parts of Spain and Turkey as well as along the north coast of Africa. Another reason may be that these are arid areas with high surface reflection, where both the AATSR and MODIS retrieval algorithms are likely to encounter problems. Over more central parts of Europe the ratio is generally closer to unity. Apparently AATSR strongly underestimates the AOT compared to MODIS over the Po Valley, where the ratio of the annual means is around 0.5. However, the AATSR and AERONET compare well for the ISDGM AERONET station in the Po Valley: the correlation coefficient is 0.89 (Table 4.1) and the AOT values are very similar (0.24 for AERONET versus 0.23 for AATSR). In contrast, MODIS significantly overestimates the AOT (0.43 versus 0.24 for the ISDGM AERONET station). Hence the low ratio of the AATSR AOT and MODIS AOT_F can be ascribed to overestimation by MODIS. Hence the low ratio between the AATSR AOT and MODIS AOT_F in the Po Valley largely reflects the overestimation of MODIS in that region. The reasons for these discrepancies need to be further investigated.

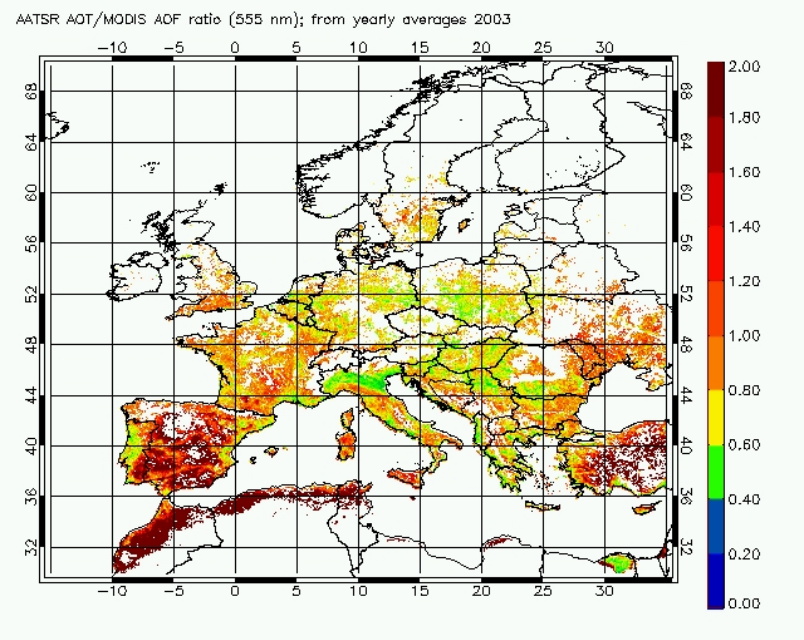

Figure 4.4 Map of the ratio of the yearly average AOT from AATSR and the yearly average AOT_F from MODIS.

In Figure 4.5, domain-averaged AATSR AOT/MODIS AOT_F ratios are presented as a function of month. The solid line shows the ratio averaged over all 0.1^o by 0.1^o grid cells within the full European domain with monthly data from both satellite instruments. The dashed line shows the corresponding curve for the region centred around the Benelux (49-55 ^{o}N, 0-10 ^{o}E). The ratio shows a distinct seasonal cycle with a maximum value higher than 3 for December and minimum values approaching unity from March to June. The high ratio in winter is likely due to insufficient screening of cloud-contaminated or snow-contaminated pixels in the AATSR data (more than in the MODIS data). Over the Benelux region, the average ratio is higher than unity during fall/winter (similar to other areas in Europe), but decreases to values in the range 0.7-0.8 during spring/summer. From validation of MODIS data in the PARMA project, it was found that MODIS overestimates AOT and AOT_F in summer compared to AERONET, while AATSR does not show such a seasonal bias; this leads to a ratio smaller than unity in summer months.

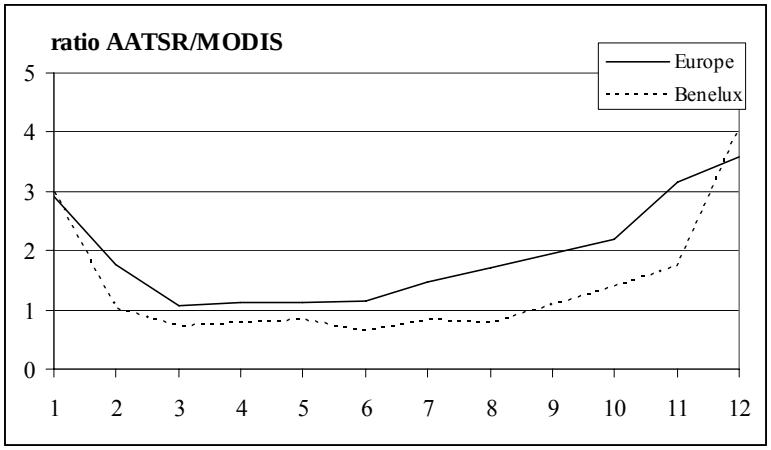

Figure 4.5 Seasonal cycle of the ratio of the monthly average AOT from AATSR and the AOT_F from MODIS. Solid line: ratio averaged over the whole European domain; dashed line: corresponding curve for the region centred around the Benelux (49-55 ^{o}N, 0 -10 ^{o}E).

5. Mapping of $PM_{2.5}$ – statistical approach

In this statistical approach, measured PM concentrations are interpolated over Europe using spatial variations that are derived from 'explanatory fields'. The method is similar to that used in the PARMA study (Koelemeijer et al., 2006a). Two explanatory fields are used: (1) the AOT fields derived from AATSR, and (2) $PM_{2.5}$ concentrations that were modelled using the LOTOS-EUROS model (Schaap et al., 2005a). The following form has been adopted to map PM:

$$PM_{fit} = a_1 AOT_{AAT} + a_2 PM_{LE} + a_3,$$

where PM_{fit} is the PM concentration obtained through fitting the AOT derived from AATSR (denoted by AOT_{AAT}), and the $PM_{2.5}$ concentrations modelled with the LOTOS-EUROS model (denoted by PM_{LE}) to AirBase measurements of $PM_{2.5}$. The coefficients a_1, a_2, a_3 are free-parameters in this model, and have been fitted through least-squares minimization of PM_{fit} (evaluated at measurement locations) and measured concentrations of $PM_{2.5}$ (or PM_{10}) concentrations. For this minimization, the Levenberg-Marquart algorithm is used. The $PM_{2.5}$ concentrations modelled by LOTOS-EUROS are also used as an explanatory field for PM_{10} concentrations, rather than PM_{10} concentrations modelled by LOTOS-EUROS. However, modelled PM_{10} does not differ much from modelled $PM_{2.5}$, as many natural sources that contribute to PM_{10} are not accounted for in the emission inventories used by LOTOS-EUROS. The fitting is performed using rural background stations that have more than 80% data capture during 2003. This leaves 142 PM_{10} stations, and, unfortunately, only eight $PM_{2.5}$ stations. The amount of stations is further reduced because AATSR yearly average data are not always available for the location of the AirBase station. Therefore, in the fitting analysis, 69 stations could be used for PM_{10}, and only six stations for $PM_{2.5}$.

Table 5.1 Fit-coefficients pertaining to fitting $PM_{2.5}$ with LOTOS-EUROS and AATSR field only, and combined. Top rows: fit forced through (0,0), bottom: a_3 is also fitted.

	$PM_{2.5}$			PM_{10}		
	a_1	a_2	a_3	a_1	a_2	a_3
LOTOS-EUROS only	0	1.31	0	0	2.09	0
AATSR only	67.2	0	0	130.0	0	0
LOTOS-EUROS and AATSR	37.5	0.59	0	34.4	1.57	0
LOTOS-EUROS only	0	0.52	7.71	0	1.51	7.31
AATSR only	30.5	0	7.02	93.3	0	6.93
LOTOS-EUROS and AATSR	26.7	0.13	6.52	-26.8	1.65	10.6

The fitting results for the coefficients a_1 (unit: $\mu g/m^3$), a_2 (dimensionless) and a_3 (unit: $\mu g/m^3$) are listed in Table 5.1. In the top rows, the fit was forced through (0,0), while in the bottom rows also the coefficient a_3 is fitted. Note that for PM_{10}, the 3-parameter fit results in a negative weighting of the AATSR field.

The correlation coefficient between the yearly average AATSR data and the PM_{10} ground based measurements is low, 0.31 (based on 69 stations), see Table 5.2. For $PM_{2.5}$, the correlation is higher, and amounts to 0.66, but it is based on a very limited number of stations (six stations only for $PM_{2.5}$). For the two-parameter fit with a_3 set equal to zero, the PM_{10} map is for 75% based on LOTOS-EUROS and for 25% on AATSR, while for $PM_{2.5}$ the weights

are about equal for both explanatory fields (45% for LOTOS-EUROS versus 55% for AATSR). The large difference in the choice for a two or three-parameter fit is apparent: the a_3 coefficient is about 7 µg/m^3 using AATSR; in the PARMA study this was about 3 µg/m^3 using MODIS (absolute values). This means that the $PM_{2.5}$ field based on AATSR depends substantially on a more or less arbitrary methodological choice and is not very robust. The results presented in the following have been obtained with a_3 equal to zero, as this is a physically more plausible model.

Table 5.2 Error-statistics for fitting AATSR measurements of yearly average AOT and/or yearly average LOTOS-EUROS fields of $PM_{2.5}$ to observed spatial variations in yearly average concentrations of $PM_{2.5}$ and PM_{10} at rural background stations in Europe. Units: µg/m^3 (mean error, root-mean-square (RMS) error, mean absolute error). Results for a_3=0.

	$PM_{2.5}$	PM_{10}	
Mean error	-0.42	-0.91	LOTOS-EUROS only
RMS error	2.87	9.17	
Mean abs. error	2.21	6.10	
Correlation coeff.	0.51	0.51	
Mean error	-0.49	-0.26	AATSR only
RMS error	2.70	10.41	
Mean abs. error	2.38	7.63	
Correlation coeff.	0.66	0.31	
Mean error	-0.33	-0.39	LOTOS-EUROS and AATSR
RMS error	2.41	9.03	
Mean abs. error	1.94	5.88	
Correlation coeff.	0.65	0.57	

Table 5.2 shows the error-statistics when AATSR measurements of yearly average AOT and/or yearly average LOTOS-EUROS fields of $PM_{2.5}$ are fitted to observed yearly average concentrations of $PM_{2.5}$ and PM_{10} at rural background stations in Europe. This table describes, in a statistical sense, the difference between observed PM levels and PM_{fit}. The mean errors are - by definition - close to zero, as this is minimized during the fitting procedure. The results suggest that the AOT field better captures the spatial variation in measured $PM_{2.5}$ than the modelled $PM_{2.5}$ fields. However, the fitting procedure for $PM_{2.5}$ is based on only six stations. An analysis based on more $PM_{2.5}$ rural background stations (i.e., an analysis for more recent years) would be necessary to investigate whether these preliminary findings holds in a more general sense. By using both explanatory fields instead of a single field for fitting $PM_{2.5}$, the errors reduce by 10-20%. However, the correlation coefficient does not improve compared to the value of 0.66 found on the basis of the AATSR field alone, and remains significantly lower than the value of 0.82 obtained within the PARMA project on the basis of a two-parameter fit of MODIS and LOTOS-EUROS fields to $PM_{2.5}$ measurements from a larger – but still very limited – number of stations.

Table 5.3 Yearly average values of measured and modelled $PM_{2.5}$, AOT, and fitting results for $PM_{2.5}$ using LOTOS-EUROS (LE), AATSR, and both LOTOS-EUROS and AATSR, at rural background stations in 2003.

Station	Technique	lat	lon	Meas. $PM_{2.5}$	Model $PM_{2.5}$	Meas. AOT	Fitted $PM_{2.5}$		
							LE only	AATSR only	LE and AATSR
DE0002R	gravimetry	52.8	10.8	16.5	10.1	0.26	13.2	17.6	15.8
DE0003R	gravimetry	47.9	7.9	10.2	9.9	0.19	13.1	12.8	13.0
DE0004R		49.8	7.1	13.8	10.6	0.15	13.9	10.0	11.9
DE0737A	β-absorption	49.3	7.8	12.5	9.2	0.15	12.1	10.3	11.2
GB0036R	TEOM	51.6	-1.3	11.8	10.8	0.21	14.2	13.8	14.1
PT0128A	β-absorption	39.2	-8.3	9.9	4.4	0.11	5.7	7.3	6.7

Our primary interest in this study is mapping $PM_{2.5}$, hence the discussion is limited to $PM_{2.5}$ in the remainder of this section. Table 5.3 lists the measured $PM_{2.5}$ and fitted $PM_{2.5}$, as well as the values of the explanatory variables at these locations. The applied calibration factors applied to the measurements are unknown for $PM_{2.5}$. Figure 5.1 shows the fitted fields for $PM_{2.5}$, using only LOTOS-EUROS as explanatory variable, using only the AOT field from AATSR as explanatory variable, and using both explanatory fields. It can be observed that, comparing the two top maps, the large scale patterns show substantial differences. It is apparent that the modelled field shows larger spatial contrasts between clean and polluted regions, and also cities are more clearly distinguishable in the modelled map. As noted above, the fitted map using both explanatory fields (bottom) mostly resembles the features of the AOT map, but large cities are more clearly present only because these are very clearly distinguishable in the modelled map.

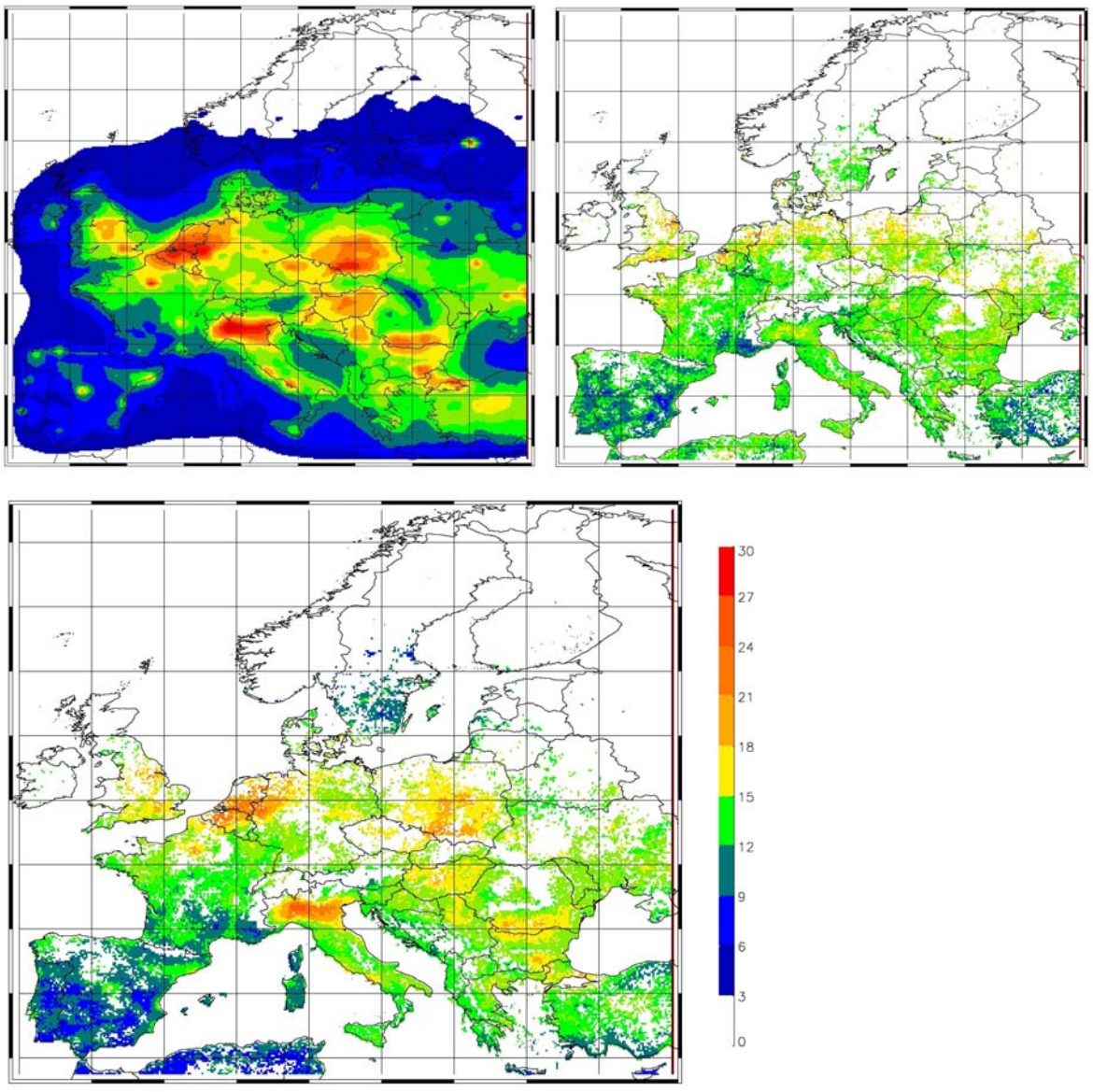

Figure 5.1 Fitted fields for $PM_{2.5}$ using only LOTOS-EUROS as explanatory variable (top left), using only the AOT field as explanatory variable (top right), using both explanatory fields (bottom, large). For these map, the fits were forced through (0,0). All maps have the same colour scale.

In Figure 5.2 the resulting $PM_{2.5}$ map is compared with the corresponding map obtained on the basis of the AOT_F from MODIS instead of the AOT from AATSR as part of the PARMA project. Over large parts of Spain, Turkey, and along the northern coast of Africa the use of AATSR instead of MODIS data results in significantly larger $PM_{2.5}$ levels. Over more central parts of Europe lower values are obtained with AATSR compared to MODIS. This is most pronounced over regions of large-scale pollution, such as over Poland and over the Po Valley in Northern Italy, where the difference can be as high as 40%. The reasons for the discrepancies between AATSR and MODIS have been discussed in chapter 4.

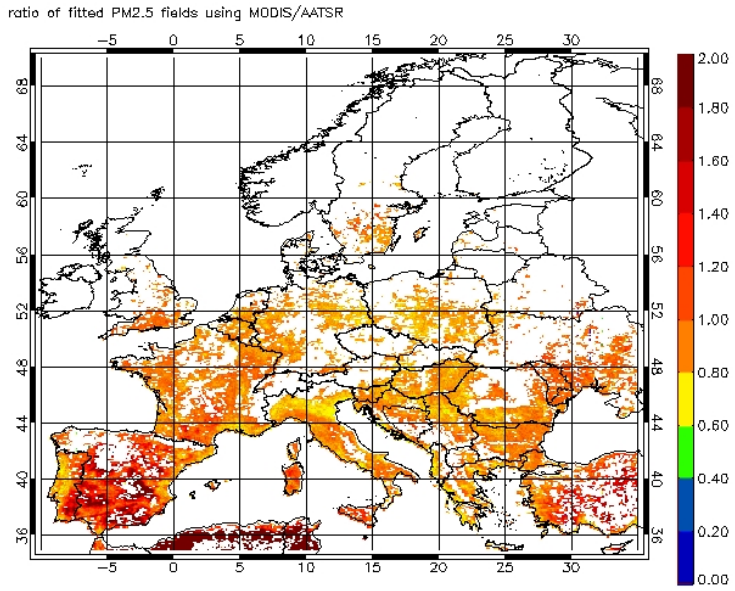

Figure 5.2 Map of the ratio of the yearly average $PM_{2.5}$ field obtained in this study from a two-parameter fit using the AOT from AATSR, and the corresponding field obtained within the PARMA project using the AOT_F from MODIS. In both cases the $PM_{2.5}$ field from LOTOS-EUROS is used as the second explanatory field.

6. Mapping of $PM_{2.5}$ – assimilation approach

The extensions made to the LOTOS-EUROS model during this project are described in section 6.1. Model results for PM_{10} and $PM_{2.5}$ in 2003, as well as individual aerosol components (secondary inorganics, organic carbon and elemental carbon) are validated using EMEP measurements in section 6.2. The assimilation results for 2003 (AATSR data) and August 1997 (ATSR-2 data) are described in sections 6.3 and 6.4, respectively. August 1997 is added to allow a comparison between AOT retrievals from AATSR and ATSR-2.

6.1 Extensions to the model system

The LOTOS-EUROS modelling system used here is described in Appendix A. Here, we present improvements made during the project, which is aimed at developing the possibility to perform simulations on a higher resolution. To that end, the model has been adapted such that at present, the system is able to simulate on resolutions ranging from 1.0 by 0.5 degree (50x50km^2) to 0.125 by 0.0625 (6x6 km^2). These higher resolutions also put additional demands to the input data for the model (meteorology, emissions, surface characteristics). At the moment, the meteorological data that are not yet available on the highest resolution, and are therefore interpolated. A limiting factor is the availability of emission data on this resolution, which are not yet available for the whole of Europe. Another important input parameter is the land use cover over Europe. During this study the land use database was updated. The starting point was the official Corine/Phare Land Cover Data from the EEA (EEA, 2000), which was completed for the full European domain by Smiatek (FI-Garmisch Partenkirchen) using (mainly) the Pelinda data base (De Boer et al., 2000). The database has a resolution of 0.0166x0.0166 degrees which is aggregated to the required resolution during the start-up of a model simulation. The land use database has the following categories:

```
1     Urban areas
2     Agriculture
3     Grassland
4     Deciduous forest
5     Coniferous forest
6     Mixed forest
7     Water
8     Marsh or wetland
9     Sand, bare rocks
10    Tundra
11    Permanent ice
12    Tropical forest
13    Woodland scrub
```

In Figure 6.1 the land use data for the Netherlands and Europe as a whole are shown. In the framework of another project, the Corine/Smiatek data base has been enhanced using the tree species map for Europe made by Koeble and Seufert (2001), who also used Corine as a basis. This data base contains 115 tree species, on a grid of 1x1 km^2, with coverage per grid. In parts of the area, especially Russia, the Koeble tree map gives no information. We started with the Corine/Smiatek land use database, and filled this in with the tree data, when the tree database has no information; the three Corine forest categories are maintained. So, the full tree data base contains 115+3 categories. The information on the tree species has been

incorporated as it enables to calculate the biogenic emissions of terpenes, which are thought to be important precursors for secondary organic aerosol (SOA) formation, and thus organic carbon levels. However, due to time constraints, in this study secondary organic aerosol could not yet be taken into account in the actual calculations.

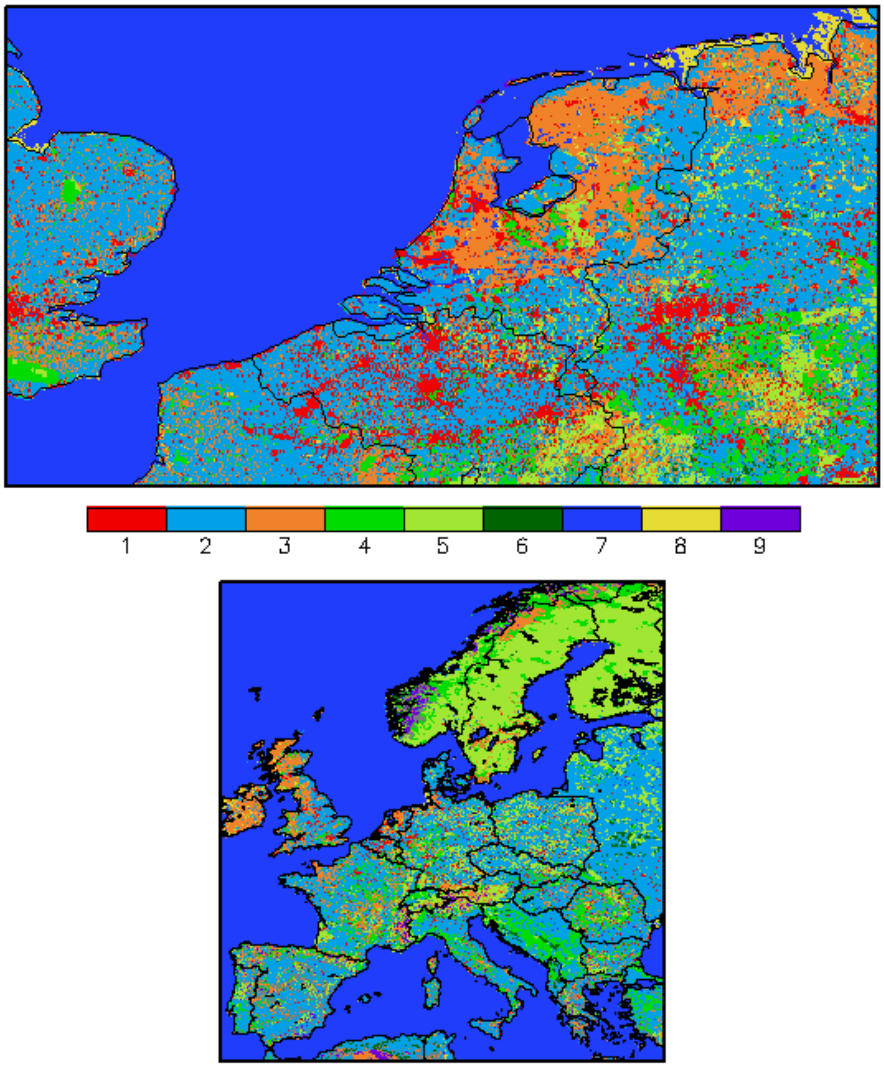

Figure 6.1 High resolution land use database for Europe. Categories are listed in the main text.

The LOTOS-EUROS model system has been adjusted to be able to run in a zoom mode at a resolution of 0.125° x 0.0625°, which corresponds to a horizontal resolution of ~6x6 km^2. The available anthropogenic and biogenic emissions have been regridded onto this model grid. The meteorological data used as input for the model have been interpolated to get the higher horizontal resolution needed. For these simulations the model domain was limited to 42.5°N to 60°N and 5°W to 30°E covering the central part of Europe. This domain was chosen to cover some highly industrialised areas (Po Valley, Ruhr area, Poland) and regions where most ground-based measurements are available. Figure 6.2 shows for this high resolution run two fields for AOT. The results show the ability of the LOTOS-EUROS model to perform runs on a high resolution of ~6x6 km^2.

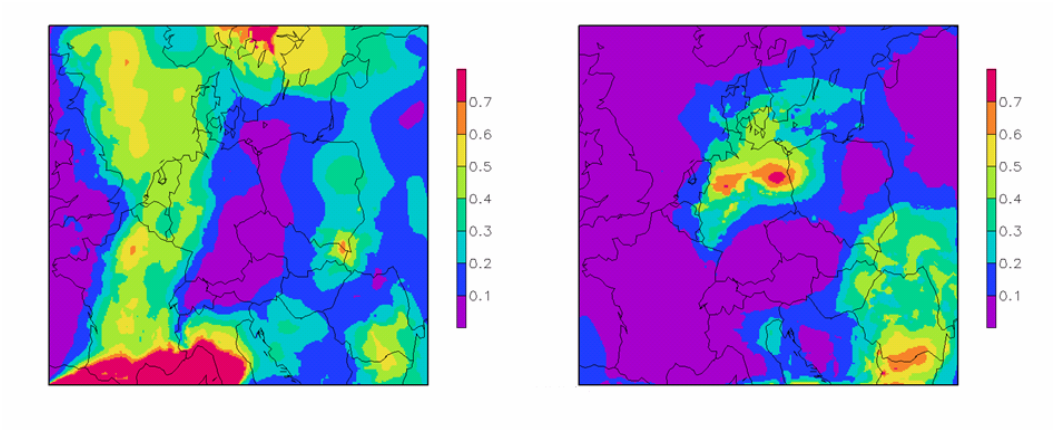

Figure 6.2 Total AOT calculated by the model at 25 July and 4 August, 2003.

6.2 Model results for PM in LOTOS-EUROS in 2003

6.2.1 PM_{10} and $PM_{2.5}$

The LOTOS-EUROS model calculates the hour-by-hour variation in aerosol concentrations over Europe. The representation of PM in the model is:

$PM_{2.5} = SO_4 + NO_3 + NH_4 + EC + OC + PPM_{fine} + SS_{fine}$
$PM_{10} = PM_{2.5} + PPM_{coarse} + SS_{coarse}$

In these equations, PPM_{fine} and PPM_{coarse} are the anthropogenic primary emitted PM with a diameter smaller than 2.5 micrometer and between 2.5 and 10 micrometer, respectively, not being Elemental Carbon (EC) or Organic Carbon (OC). In practice, this PPM consists of contributions from traffic (wear of tyres, brakes, roads) and industry (related to combustion and non-combustion). SS_{fine} and SS_{coarse} are the sea salt contributions in the corresponding size ranges. Thus, PM_{10} and $PM_{2.5}$ are the sum of the individual model components. In Figure 6.3 the modelled field of PM_{10} for 2003 is depicted. PM_{10} is shown because many measurements are available in the AirBase database to compare with. Presently, in the model, the difference between PM_{10} and $PM_{2.5}$ stems mainly from the fact that the coarse mode sea salt (SS) particles are taken into account. Also, there is a slight contribution of PPM_{coarse} to PM_{10}. Dust and secondary organic aerosol (SOA) are not included in the current model. This feature is illustrated in the comparison with observed PM_{10} data. The model underestimates the measured PM_{10} concentrations by about 40% on average. A large part of the underestimation is caused by a lack of particles in the coarse mode, like mineral dust.

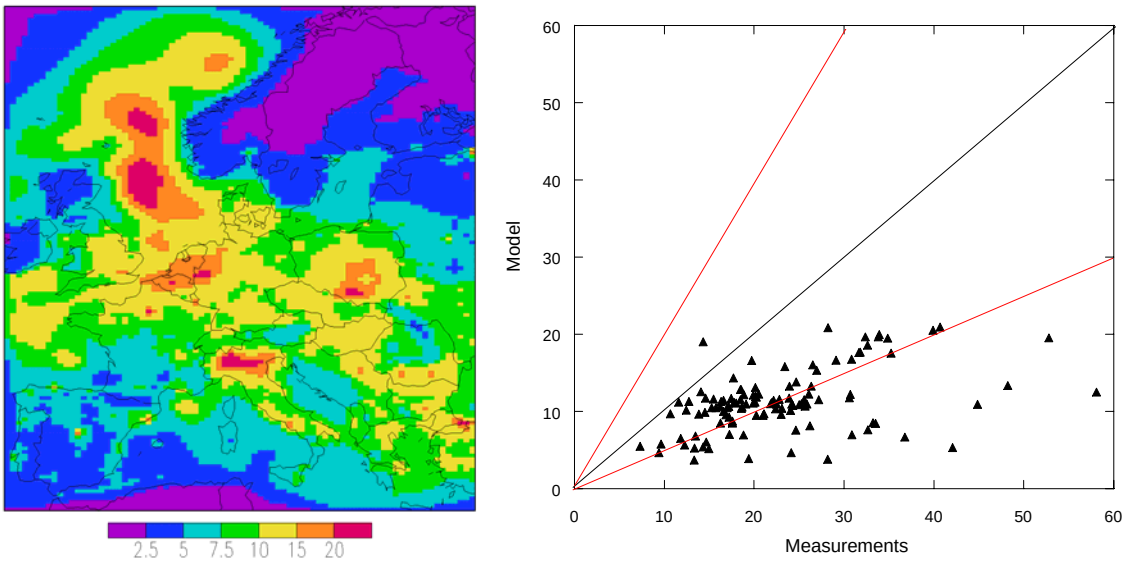

Figure 6.3 Modelled PM_{10} field over Europe (left) and comparison between modelled and measured PM_{10} levels for the AirBase stations (right). Yearly averages for 2003 are shown.

For $PM_{2.5}$, only few data points in 2003 are available to compare with. This comparison is shown in Table 6.1 for the annual average concentration for a number of regional sites spread over Europe. Except for AT0002R (in Austria), the model underestimates the $PM_{2.5}$ measurements by about 10-40%. The average underestimation is lower than for PM_{10}. The spatial correlation is 0.88 for the modelled field, which hints at a good representation of the large scale gradients in the model. To investigate the reasons for the underestimation we present the comparison to observations for the individual components as well (see sections 6.2.2 and 6.2.3).

Proper validation of the modelled $PM_{2.5}$ fields is not only restricted by the low number of available ground based measurements in 2003 but also by the quality of the ground based measurements of $PM_{2.5}$. There are several difficulties in measuring $PM_{2.5}$ and PM_{10}, which leads to a large uncertainty in the measurements, as was discussed in section 2.2.

Table 6.1 Comparison of modelled and measured $PM_{2.5}$ concentrations for 2003.

Station	lat	lon	Meas. $PM_{2.5}$	LE model	Residue model
AT0002R	47.8	16.8	24.7	10.9	13.8
DE0002R	52.8	10.8	16.5	9.1	7.4
DE0003R	47.9	7.9	10.2	8.6	1.6
DE0004R	49.8	7.1	13.8	9.4	4.4
DE0737A	49.3	7.8	12.5	8.0	4.5
GB0036R	51.6	-1.3	11.8	8.9	2.9
GB0617A	51.5	0.6	12.5	10.9	1.6
IT0004R	45.8	8.6	28.5	15.4	13.1
NO0001R	58.4	8.3	5.0	2.2	2.8
NO0099R	58.1	6.6	7.3	3.0	4.3
SE0011R	56.0	13.2	10.5	6.0	4.5
SE0012R	58.8	17.4	4.8	3.5	1.3

6.2.2 Secondary inorganic aerosol

The verification of the sulphur dioxide and sulphate concentrations to EMEP observations shows that the model slightly overpredicts SO_2 and slightly underpredicts the sulphate concentrations (see Figure 6.4). The largest uncertainty in the modelling of sulphate is thought to be the conversion between SO_2 and SO_4 in the water phase (clouds, fog, aerosol).

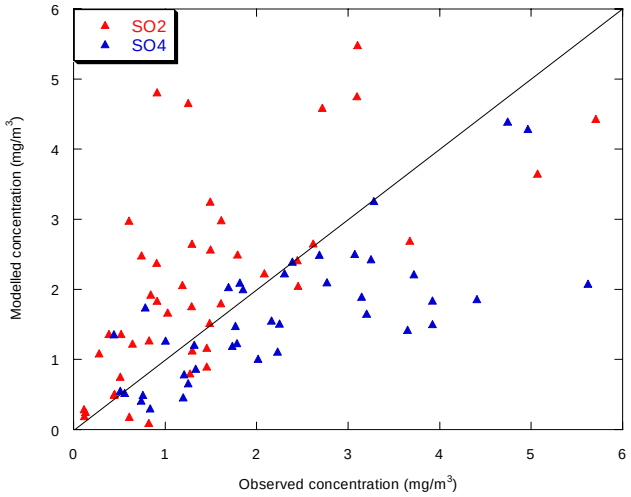

Figure 6.4 Comparison between modelled and measured SO_2 and SO_4 concentrations; yearly averages for 2003 are shown.

For nitrate the validation is restricted to only six stations, four of which are located in the Netherlands. It turns out that the model overestimates nitrate in the Netherlands. However, since the validation is largely restricted to the Netherlands, this conclusion cannot be drawn for the whole of Europe. We have used the total nitrate observations (sum of nitrate and nitric acid) to give a broader perspective to the performance for the European situation (see Figure 6.5). For total nitrate we find a very nice correspondence with all data around the one-to-one line. Ammonium is slightly overestimated, which may hint at a too high nitrate concentration at these locations. For all SIA components (sulphate, nitrate and ammonium) the average temporal correlations are about 0.5, and the spatial correlations are about 0.75. This demonstrates that the model is capable to simulate SIA distributions in Europe.

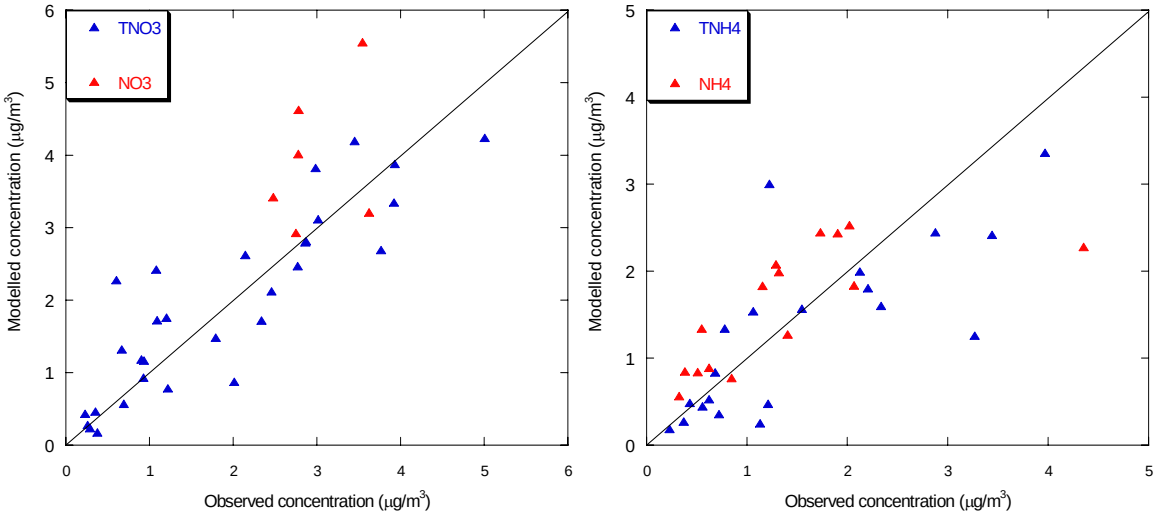

Figure 6.5 Comparison between modelled and measured total nitrate (left) and total ammonium (right) concentrations; yearly averages for 2003 are shown.

6.2.3 Carbonaceous particles

We have used the EMEP EC/OC campaign to verify our modelled concentrations for carbonaceous components. The EMEP EC/OC campaign was performed from summer 2002 to summer 2003 during which every sixth day a sample was collected at 12 sites within the LOTOS-EUROS domain. We compare the averaged measured values to the collocated model values in Figure 6.6. As the split between EC and OC is under discussion and variable among analysis methods, the total carbon comparison is a good measure to look at the overall performance. From Figure 6.6 it is obvious that we systematically underestimate total carbon levels in Europe. Looking at the split between EC and OC we can see that both components are underestimated. However, the underestimation is more pronounced for OC than for EC. For EC, which is a purely primary component, the reason for the underestimation may be due to (a combination of) too low emission estimates, too short lifetime or uncertainties in the EC-OC split in the analysis. For a detailed discussion on EC we refer to Schaap et al. (2004). For OC, the uncertainties in the analysis method are probably not that important because OC dominates the total carbon. However, uncertain emission estimates and the potentially significant contribution of secondary organic material are the likely candidates to explain the underestimation. In conclusion, the validation of the model for individual components (SIA, EC, and OC) shows that it is suited to simulate aerosol distributions in Europe.

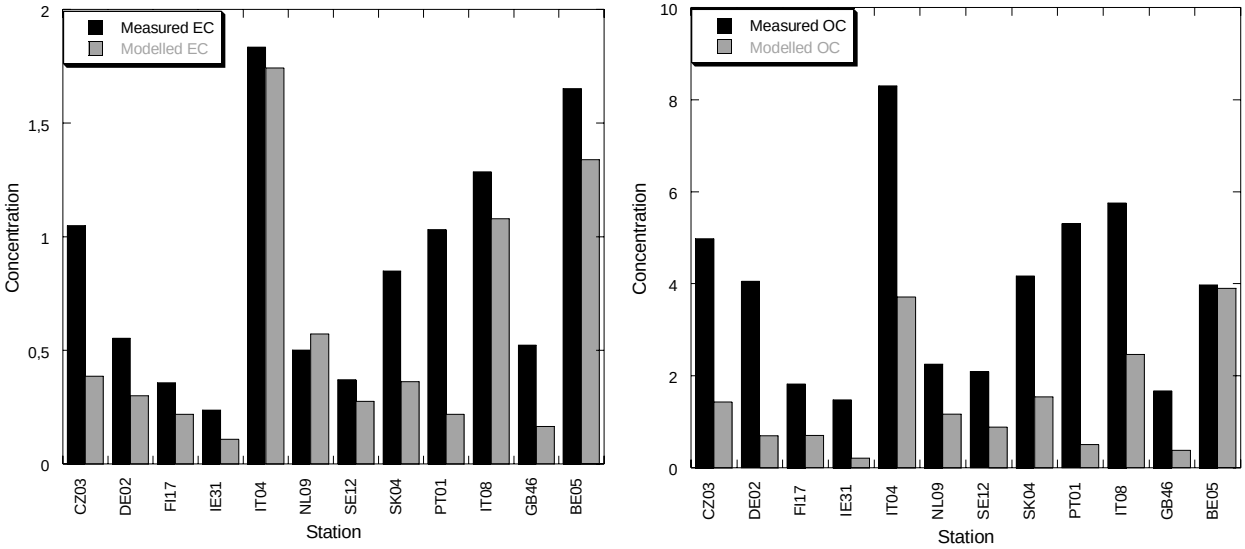

Figure 6.6 Comparison between modelled and measured EC (left) and OC (right) concentrations; yearly averages for 2003 are shown.

6.3 Assimilation experiment for summer 2003

6.3.1 Assimilation approach

Observations of aerosol optical thickness (or any other component) consist of data that are irregularly distributed in space and time. Data assimilation allows the calculation of continuous fields in space and time from observations that are irregularly distributed. Data assimilation consists of making a best estimate of the state of the atmosphere on the basis of observations and a model prediction of the atmospheric state, both of which have associated errors. Data assimilation basically defines a new atmospheric state by making a weighted average of the observed and modeled state in an intelligent and statistically sound way. Hence, if a model value is more uncertain than an observed value, more weight will be put on

the observation, and the assimilated value will tend to get closer to the observed value and vice versa (see Figure 6.7).

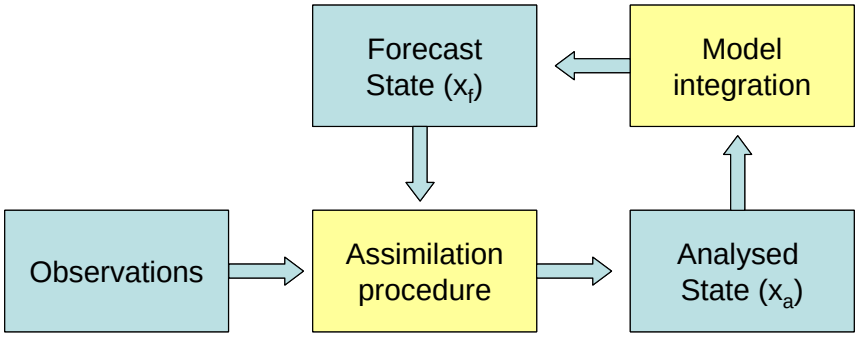

Figure 6.7 Schematic representation of the data assimilation procedure.

In this study an ensemble Kalman filter was applied to assimilate the AOT retrievals within LOTOS-EUROS. The uncertainties involved with the modelled and retrieved AOT values determine the weights assigned to the measured and calculated values. With a Kalman filter there is no need to specify the model uncertainties as they are determined by the range of modelled states of the ensemble members. Hence, the specification of the noise influences the weights and therewith the results of the procedure. In the present study, an ensemble of only 15 ensemble members was used to speed up calculation time. To generate an ensemble, random noise was added to the emissions of NO_x, SO_x, VOC, NH_3 and particles, and to the dry deposition velocities. The noise varies per time step, and has no regional variability. All noise factors were applied with a mean of 1 and a standard deviation of 0.25. Hence, the vast majority for the factors are within the range of 0.5 to 1.5. All noise factors were set after an assimilation step and held constant until the next assimilation step.

The AATSR and ATSR-2 overpasses take place around 10:00 and 10:30 hours local time every third day, respectively. In the model the analysis is performed at 12:00 hours GMT and all ensemble members have disturbed emissions for the 24 hours between overpasses. The perturbation is constant during these 24 hours. At noon, the AOT is calculated for the grid cells for which observations are available and the state and ensemble members are updated in the analysis step.

We have applied the system to June and July, 2003. August 2003 was not selected because of an abnormally high intensity of forest fires in southern Europe, which are not included in the emission database and would disturb the assimilation experiment too much. As discussed in the previous chapters the AATSR data for 2003 may to a large extent be influenced by cloud contamination and, after rigorous selection of valid data, not enough information was left to assimilate in the LOTOS-EUROS model. This is in contrast to earlier studies where the scientific retrieval algorithm was used. Hence, also the AOT retrieval results for 1997 obtained from ATSR-2 (Robles González et al., 2003) were analysed, in order to assess the performance of the assimilation method if more and higher quality data are available. For both retrieval algorithms (i.e., the 'scientific' algorithm applied to August 1997, and the algorithm applied to 2003 data using automatic cloud detection) an uncertainty estimate of sigma = ±0.05± 0.20*AOT was used. This estimate equals that of the MODIS instrument used in the PARMA study. For two reasons this uncertainty estimate was chosen: 1) the evaluation against AERONET showed more or less similar RMS-errors for AATSR as compared to MODIS and 2) to be able to compare the influence of data availability (keeping

the uncertainty constant allows a comparison between AATSR and ATSR-2 / MODIS in this respect, bearing in mind that ATSR-2 has more data available for August 1997 due to many clear-sky situations).

6.3.2 Assimilation results for the AOT

In the upper left panel of Figure 6.8 the retrieved AOT values for 4 June 2003 are shown. There are two swaths over Europe, one over Ireland and one over Central Europe (Sweden, Poland, Germany, Italy). The swath over Ireland shows only a small number of available AOT data. On the other hand, the swath over Central Europe shows a large area with available AOT data, and shows a band of enhanced, moderately high, AOT over northern Germany, Poland and Sweden. Furthermore, a secondary maximum is found in the Po Valley, Italy. The modelled AOT for the simulation without assimilation (left) and with assimilation (right) are shown in the middle panels. In this case, the modelled AOT does not underestimate the retrieved values. Assimilation affects the calculated AOT in Central Europe. For 4 June the assimilation results in a better representation of the details in the patterns in Central Europe, effectively reducing the AOT over Poland. As shown in the lower panels of Figure 6.8 the absolute residue is lowered in this area. In regions close to the domain edge, such as Ireland, the assimilation scheme is not able to lower the discrepancy between the model and observation.

In Figure 6.9 the assimilated AOT field for 26 July 2003 is shown. At this day high AOT values are retrieved for a swath over Western Europe (Portugal and the UK) as well as over Central and Eastern Europe. Except over the Baltic States, the model without assimilation underestimates the retrieved AOT. The assimilation experiments are able to get closer to the observations in both the northern and southern part of the swath over Central Europe. This is not the case over Portugal where all model estimates give AOT values close to zero.

These examples are two reasonable cases that show that the system works. However, the quality of the data used as input to the system is of utmost importance, as is shown in the remainder of this section.

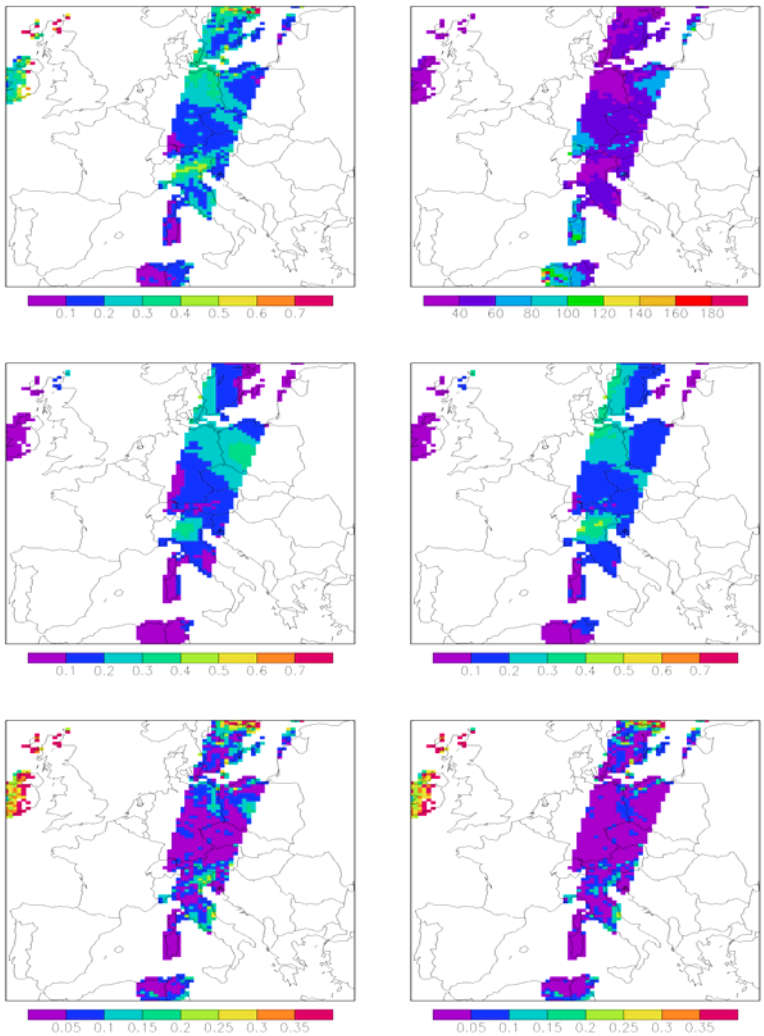

Figure 6.8 AOT assimilation results for 4 June 2003. The upper left panel shows the retrieved AOT value. The corresponding relative standard deviation (%) is shown in the upper right panel. The middle left panel shows the modelled AOT values (without any assimilation) whereas the middle right panel shows the AOT in the assimilation experiment. The lower left and right panels show the residues for the model run and the assimilation experiment, respectively.

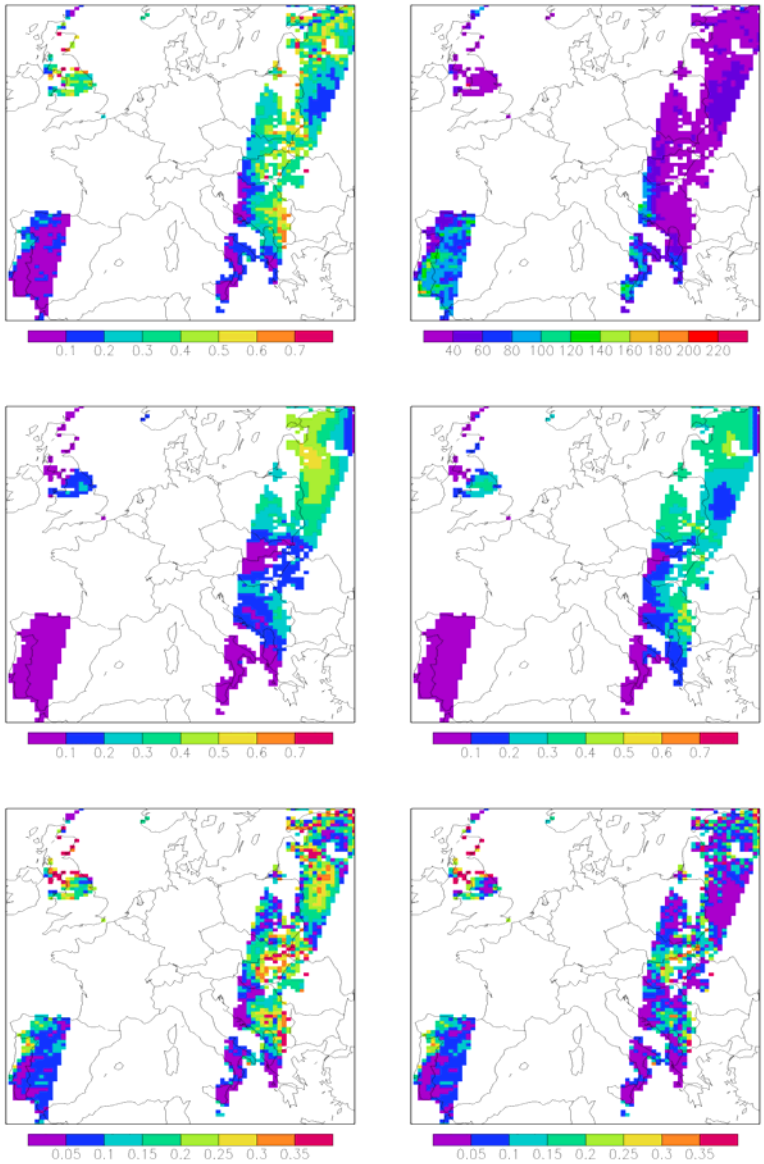

Figure 6.9 AOT assimilation results for 26 July 2003. The upper left panel shows the retrieved AOT value. The corresponding relative standard deviation (%) is shown in the upper right panel. The middle left panel shows the modelled AOT values (without any assimilation) whereas the middle right panel shows the AOT in the assimilation experiment. The lower left and right panels show the residues for the model run and the assimilation experiment, respectively.

In Figure 6.10 we summarize the influence of the assimilation for the whole period. In this figure the average retrieved AOT is compared to the modelled and assimilated ones. Hence, we present averages for the swaths of the satellite, which results in a composite map. On the left the composite of the AATSR AOT shows the spatial trend with an increase from south to north as discussed in Chapter 3. The modelled AOT shows a pattern over Europe with an area of high AOT in Southeastern Europe, extending to Poland, Germany and the Benelux. The model yields pronounced secondary maxima in the Po Valley and in the UK. In the model the AOT trails off to less polluted and remote regions such as Ireland, Scandinavia and the Iberian Peninsula.

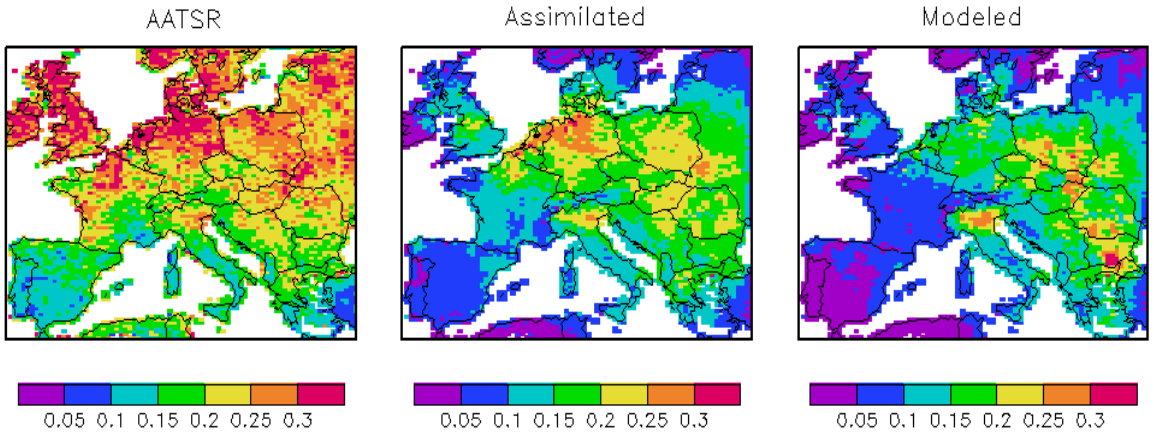

Figure 6.10 Composite map of retrieved (left), assimilated (middle) and modelled AOT fields for June-July, 2003.

The composite map for the assimilation shows a few peculiar changes compared to the modelled composite. First of all, near the edge of the domain the assimilation is not effective. This feature is well known from the PARMA project and caused by the fact that the boundary conditions have not been perturbed. More importantly, the assimilation has made the modelled maxima in Southeastern Europe and the Po Valley less pronounced whereas it has increased the AOT in a band over northern Central Europe (Benelux, Germany, Poland). Thus, except the areas near the domain edges, the assimilation incorporates the south to north gradient observed in the retrievals. Although it indicates a successful assimilation, we are not sure how to appreciate the changes due to the assimilation as we have shown that the retrievals show a large percentage of invalid AOT values.

6.3.3 Validation of the assimilated AOT

In this section, we assess the assimilation results against AERONET AOT observations. In Figure 6.11 the modelled and assimilated monthly mean AOT are compared to those of AERONET. Obviously, the model underestimates the AOT. Assimilation of the AATSR data, which have no bias compared to AERONET, leads to higher mean AOT values.

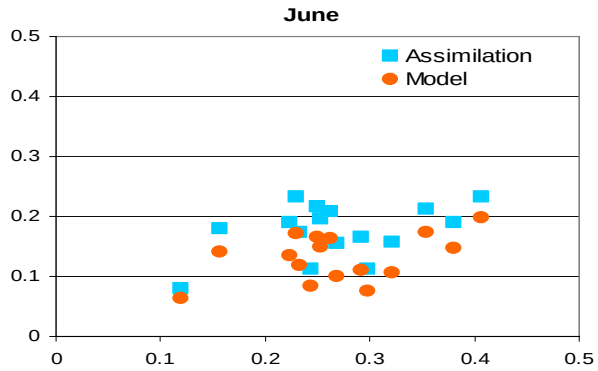

Figure 6.11 Comparison between modelled/assimilated and measured AOT data for AERONET locations in June 2003.

The day by day variability of the AOT is shown for Venise (Italy) and Oostende (Belgium) in Figure 6.12. Both stations indicate that the assimilation closely tracks the modelled AOT. Occasionally, the assimilation results are pulled away from the model state but many events are missed due to the low availability of satellite retrievals to assimilate. Further, the impact of assimilation in an area has a limited influence in time (~48 hours). The correlation with the observations in Oostende does not improve, whereas it does for Venise.

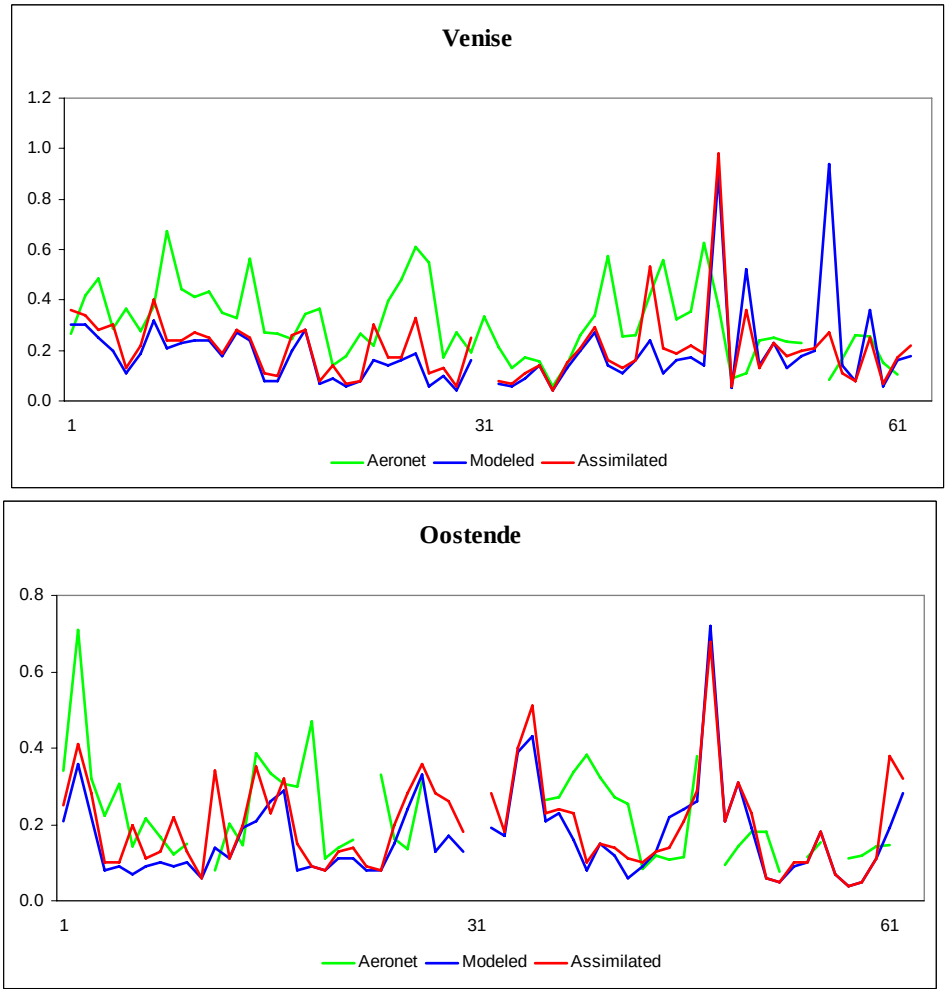

Figure 6.12 Time series of modelled, assimilated and measured AOT at the AERONET sites of Venice and Oostende (for June and July 2003).

It was found that the assimilation does not clearly improve the correlation with AERONET, which should be the case for a successful assimilation experiment. The comparison also shows that a better time resolution (more overpasses in time) would be beneficial for the assimilation experiments. Obviously, also a good estimate of the accuracy of an AOT value is mandatory. Verver et al (2006) have shown that the uncertainty estimate of the measurements influences the improvement by the assimilation process significantly.

6.3.4 Assimilation results for $PM_{2.5}$

In Figure 6.13, $PM_{2.5}$ distributions for June and July, 2003 are depicted. The left panels show the modelled distribution and the right panels show the fields after assimilation of AOT. As we showed above, the relatively low availability of observations causes modest changes in the AOT composite map. This is reflected in the $PM_{2.5}$ maps. For June the assimilation causes a modest (~1.5 $\mu g/m^3$) but systematic increase of the $PM_{2.5}$ levels compared to those modelled. However, for July there are only slight differences. Moreover, the general patterns are maintained which is also attributed to the low temporal resolution of the satellite overpasses. In conclusion, the low temporal resolution leads to limited changes in the assimilated field compared to the regular model calculation.

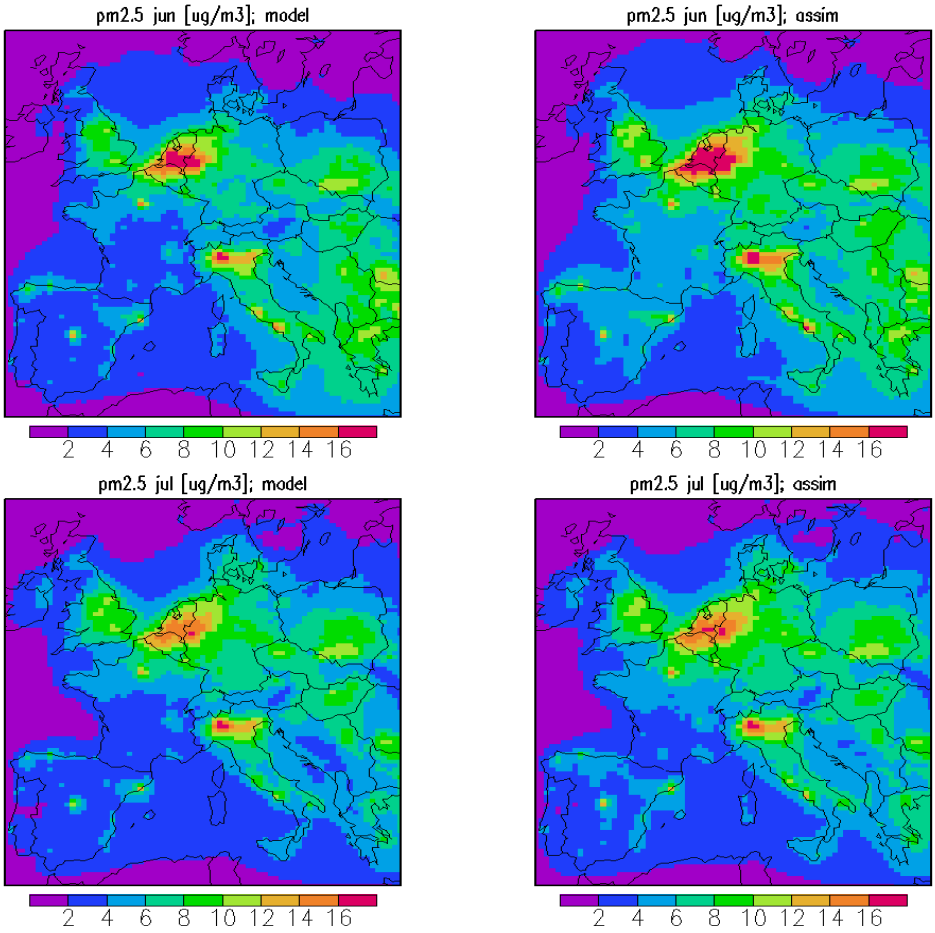

Figure 6.13 $PM_{2.5}$ fields from the model and the assimilation experiment.

6.4 Assimilation experiment for August, 1997

6.4.1 Model results without assimilation

In Figure 6.14 the total modelled AOT for August, 1997 is shown. High AOT is modelled over a band from Northwestern Europe over Central Europe to the southeast. High AOT is also modelled over the Ukraine and other countries of the former Soviet Union. Modelled average AOT exceeds 0.2 over the Ukraine, the Benelux and Southeastern Europe. Modelled AOT is lower than 0.1 in Scandinavia and Southwestern Europe, trailing off with distance from the major source regions.

Sulphate contributes most to the AOT over Europe. Over most of Europe its contribution is more than 50%. Only over areas where nitrate has its peak, the relative contribution is lower. AOT by nitrate peaks over ammonia-rich areas such as the Netherlands, Germany and Northern France. In addition, a significant contribution from nitrate to the total AOT is modelled over the relatively cool Scandinavian countries which were downwind of the European continent during a large part of August 1997. Over southern Europe the ambient temperatures were so high that nitrate formation was not favoured. It can be seen that sulphate concentrations are enhanced over Central Europe. In this region, sulphate contributions to the AOT in August 1997 are probably underestimated, as August 1997 has been simulated here using emissions for 2003, while the SO_2 emissions in especially Central Europe have decreased significantly over the last years of the 1990s.

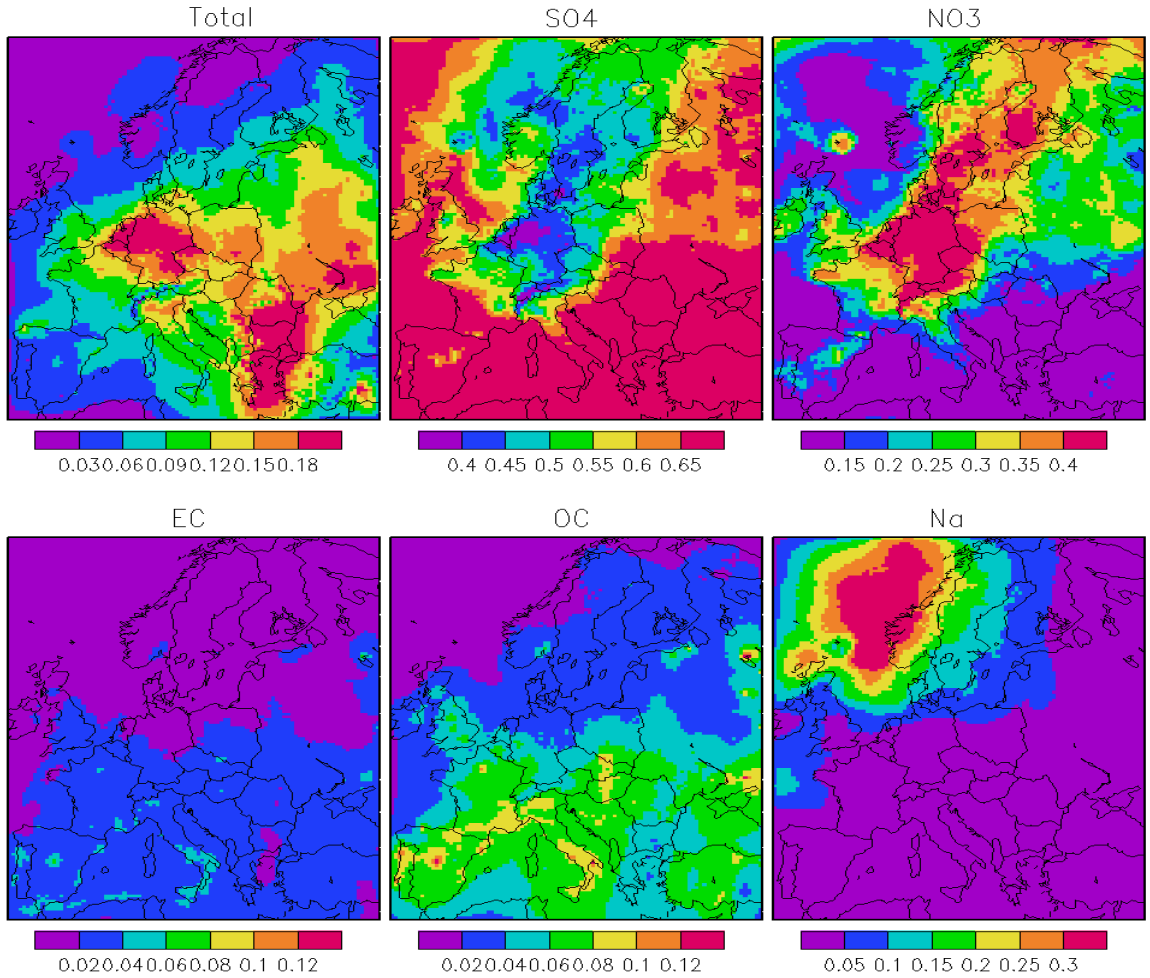

Figure 6.14 Total AOT (upper left) and the percentage contribution of each of the species. Meteorology of August 1997 is used and emissions of 2003.

Primary carbonaceous particles contribute 2-4% (EC) and 4-10% (OC) to the total AOT in this month, respectively. The relative contributions tend to peak in southern Europe. This can be explained by the lower amounts of sulphate and nitrate in this part of Europe in combination with a dense population and high emission density, in contrast to Scandinavia. Sea salt contributes significantly over the Atlantic Ocean and some coastal regions.

6.4.2 Assimilation results for the AOT

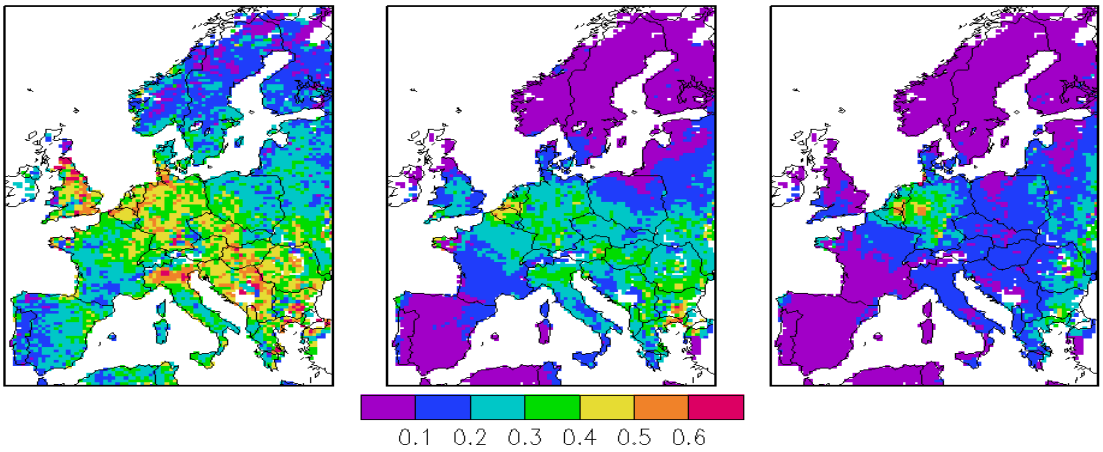

Figure 6.15 Composite map of retrieved (left), assimilated (middle) and modelled AOT fields for August, 1997, averaged over the moments of the satellite overpasses.

The composite maps for August, 1997 (see Figure 6.15) show the retrieved AOT on the left and the modelled AOT in the right panel. In these maps, averages are shown for the moments of the satellite overpasses. The modelled composite shows two maxima. These are located in Northwestern Europe and Southeastern Europe. In these regions the AOT is dominated by nitrate and sulphate, respectively. The area with relatively low modelled AOT in Central Europe (Poland) is caused by the meteorological situations during the satellite overpasses in this month, with yield low modelled AOT at times of the satellite overpass in this month. It is clear that the compilation after assimilation reflects the general patterns of the retrieved AOT much more closely, and the residual (measurement-model) is lowered significantly after assimilation.

6.4.3 Assimilation results for $PM_{2.5}$

The AOT assimilation shows a larger impact on modelled $PM_{2.5}$ concentrations for August 1997 than for 2003. Over the Central part of the domain the $PM_{2.5}$ levels increase by 1.5 to more than 3 $\mu g/m^3$ in August 1997, corresponding to an increase of 20-40%. Although the spatial patterns are maintained here as well, the gradients do show more deviations from the starting point than for 2003. The higher influence from the assimilation for August 1997 is explained by 1) the relatively high temporal resolution due to the extreme nice weather in that month and 2) the closer agreement between modelled and retrieved patterns in AOT.

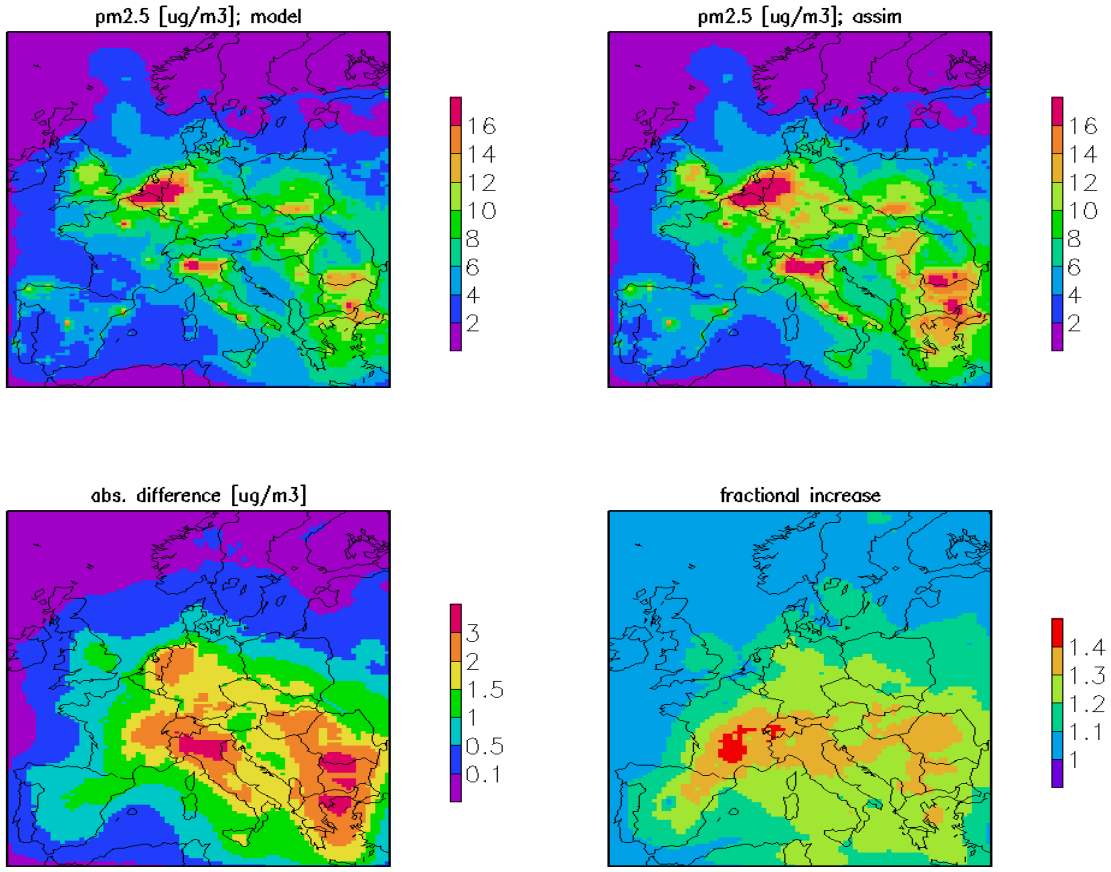

Figure 6.16 $PM_{2.5}$ distributions (August 1997) in the model and assimilation experiments (upper panels) and the absolute and relative differences in the lower panels.

7. Radiative forcing analysis

Aerosols of anthropogenic origin play a key role in changing the Earth's radiation budget. Aerosols directly scatter and/or absorb solar radiation. Indirectly, they influence the micro-physical properties of clouds and therewith their effective albedo. Over polluted continental regions the direct radiative forcing of sulphate alone can be as large as those of the combined greenhouse gases, but of opposite sign (e.g. Charlson et al., 1992; Kiehl and Briegleb, 1993). In the last decade the influence of a number of other aerosol components, like organic carbon, black carbon and mineral dust, on the radiation budget has also been shown (IPCC, 2001, and references therein). However, IPCC (2001) did not present a best estimate for the direct radiative forcing by nitrate, mostly because of a lack of reliable measurements on this semi volatile compound.

A critical assessment of nitrate observations in Europe in combination with modelling showed that nitrate significantly contributes to the aerosol radiative forcing in Northern Europe (Schaap, 2003). The radiative forcing calculations made in this project revealed that the relative importance of nitrate to total radiative forcing in Europe has increased over the last decade. The calculations for 2003 and the comparison to the situation for 1995 are presented here.

The direct radiative forcing of sulphate and nitrate for cloud free conditions was assessed using the parameterization of Van Dorland et al. (1997), which relates AOT and direct aerosol radiative forcing. These authors used optical properties for the Koepke et al. (1997) water soluble aerosol type, which includes some absorption. In fact, they implicitly assume a certain fixed mixture of different aerosol components, including some absorbing components like soot. Hence, our calculated radiative forcing values for nitrate and sulphate will actually be lower limits. However, by considering the ratio between radiative forcing from sulphate and nitrate, these errors largely cancel. The hourly AOT fields are obtained from the model simulation described above. Seasonal values for the surface albedo were taken from Matthews (1984).

Radiative forcing estimates for sulphate and nitrate presented in the literature are based on the assumption of different optical properties and various ways were used to account for water uptake. As a consequence, the radiative forcing efficiencies for sulphate for instance vary more than a factor of 3 (Adams et al., 2001). The nitrate to sulphate radiative forcing ratio, however, is relatively independent, since the optical properties of sulphate and nitrate are alike and hence largely cancel in the ratio. Therefore, the nitrate to sulphate radiative forcing ratio is most probably the most robust indicator to assess the importance of nitrate. The ratio basically gives a weighted ratio of the column burdens where the weight is determined by the solar zenith angle, which controls the fraction of the light scattered back into space. Weighting with the solar zenith angle is important as the daily cycle for sulphate is less pronounced as for nitrate (which has a clear minimum around noon when temperatures are highest).

In Figure 7.1, the nitrate to sulphate radiative forcing ratio is shown as function of season in 2003. In spring the ratio of nitrate to sulphate radiative forcing is 50% or more over most of continental Europe with equal importance over the Benelux, Germany, England, France, the Po Valley and the Alpine region. In autumn the importance of nitrate is somewhat smaller

than in spring. The maximum ratios in summer are found in the same regions as in spring and autumn. However, the thermal instability of ammonium nitrate causes the ratio to be lower especially in more remote locations. Averaged over the domain and the year the radiative forcing by nitrate is ~55% of that of sulphate. For October to March, this number is about 90%.

Comparison to 1995 (Figure 7.2, see also Schaap (2003)) shows that the radiative forcing ratio was lower in the mid-1990s. Schaap (2003) found an annual mean ratio in 1995 of ~20%, while in the winter the ratio was ~45%. Hence, we find that the importance of nitrate has increased significantly over time in Europe. This feature is caused by the decreasing trend in sulphur emissions and sulphate concentrations where nitrate levels have remained more-or-less stable despite a reduction in NO_x emissions in Europe in this period. Inter-annual variability may also contribute to the analysis. However, the average ratio of observed to modelled concentrations at the EMEP locations are only a few percent apart, indicating a relatively small uncertainty.

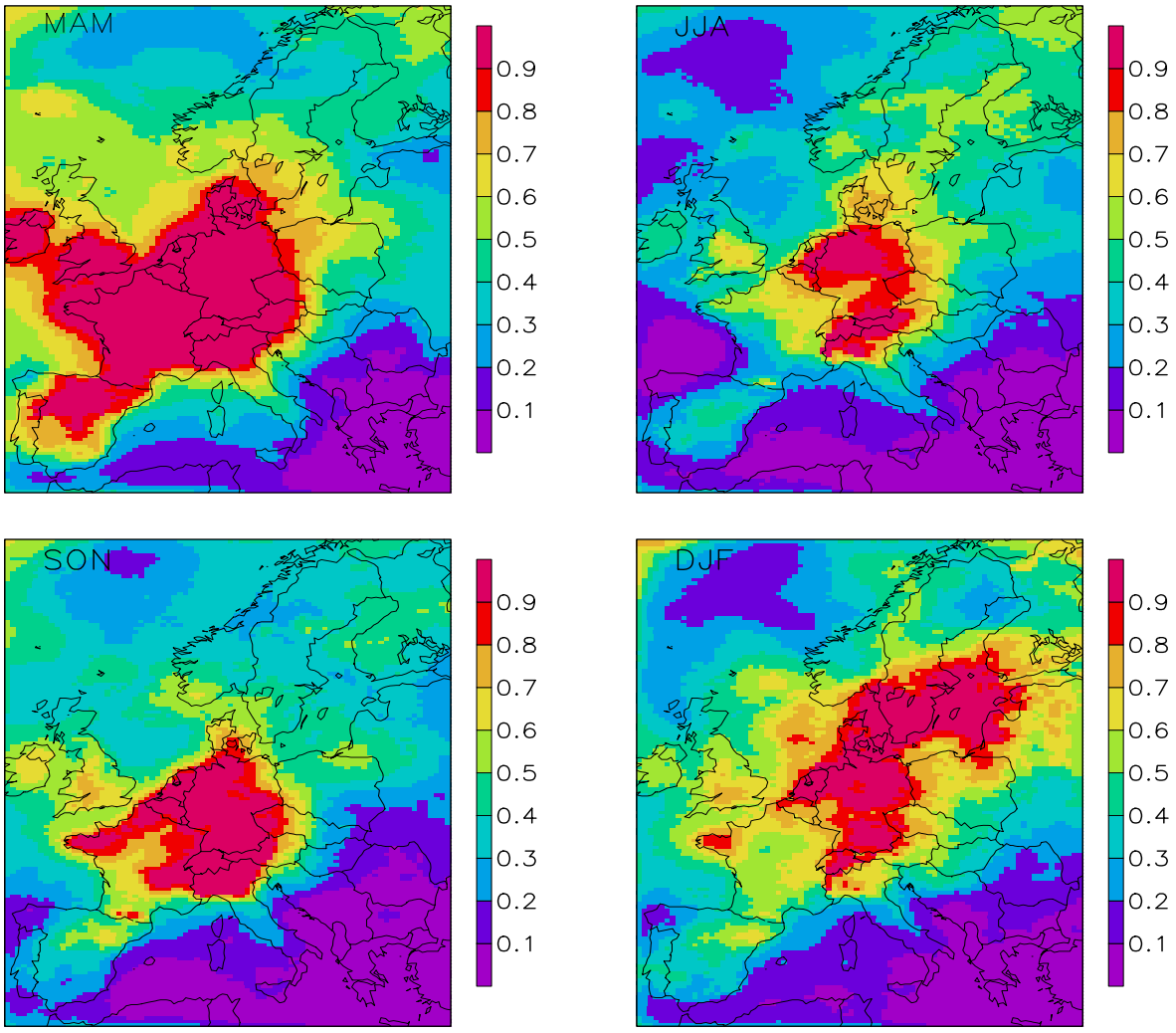

Figure 7.1 Distribution of the nitrate to sulphate radiative forcing ratio as function of season for 2003.

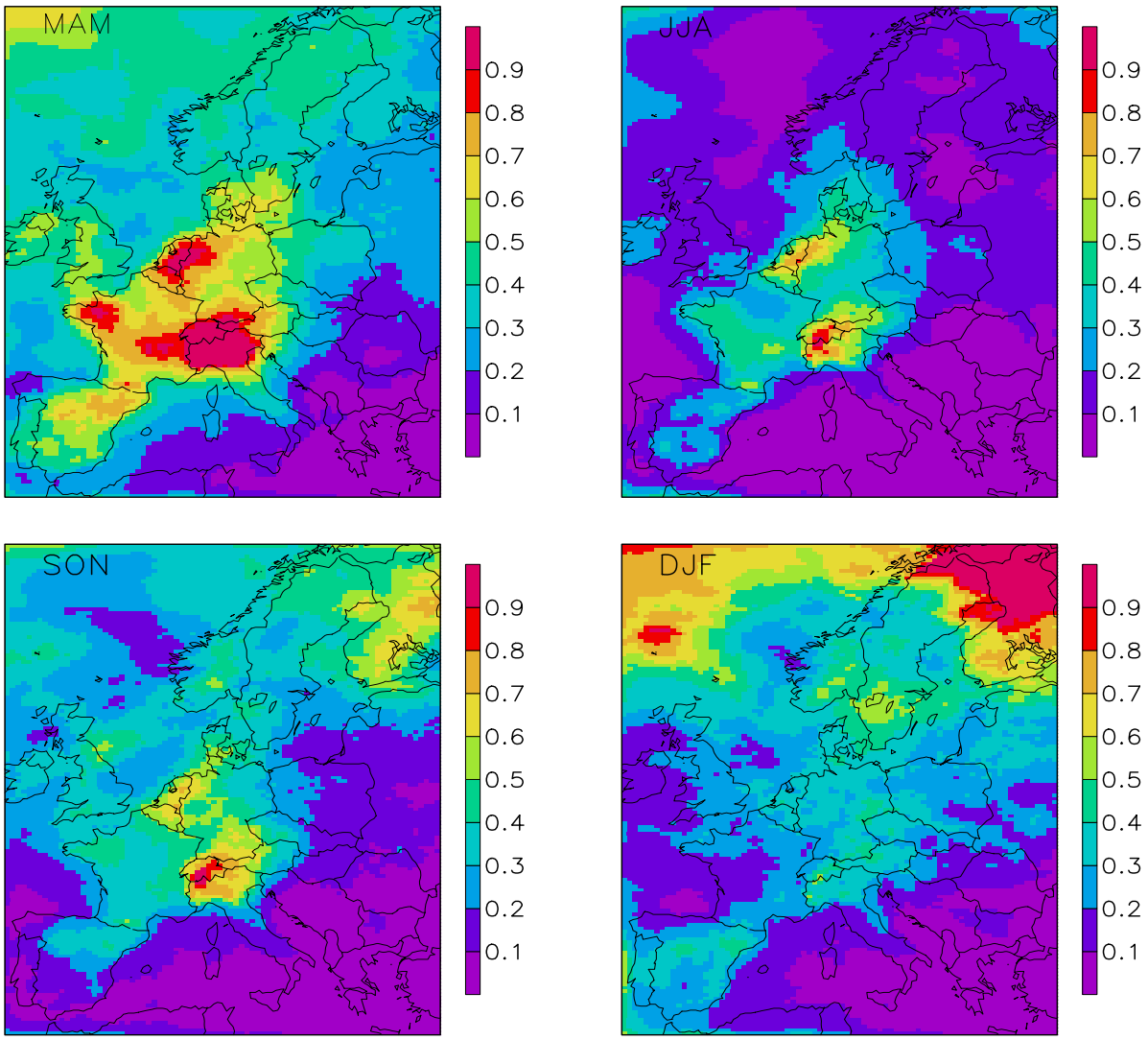

Figure 7.2 Distribution of the nitrate to sulphate radiative forcing ratio as function of season for 1995.

Verification with measurements (Figure 7.3) shows that the model is able to reproduce the basic features of nitrate and sulphate concentrations over Europe. Nitrate concentrations exceed those of sulphate in Western Europe. Based on our simulations the annual radiative forcing by nitrate is calculated to be in the order of 55% of that by sulphate, whereas for 1995 the percentage was only 20%. In the summer nitrate is found to be only regionally important, e.g. in Northwestern Europe, where the radiative forcing of nitrate equals that by sulphate. In the winter radiative forcing due to nitrate over Europe is about equal to that due to sulphate. These results are in agreement with estimates based on measured data (Ten Brink et al., 1997; Schaap et al., 2002). Overall, radiative forcing due to nitrate is significant and gaining importance compared to sulphate and should thus be taken into account to estimate the impact of regional climate change in Europe.

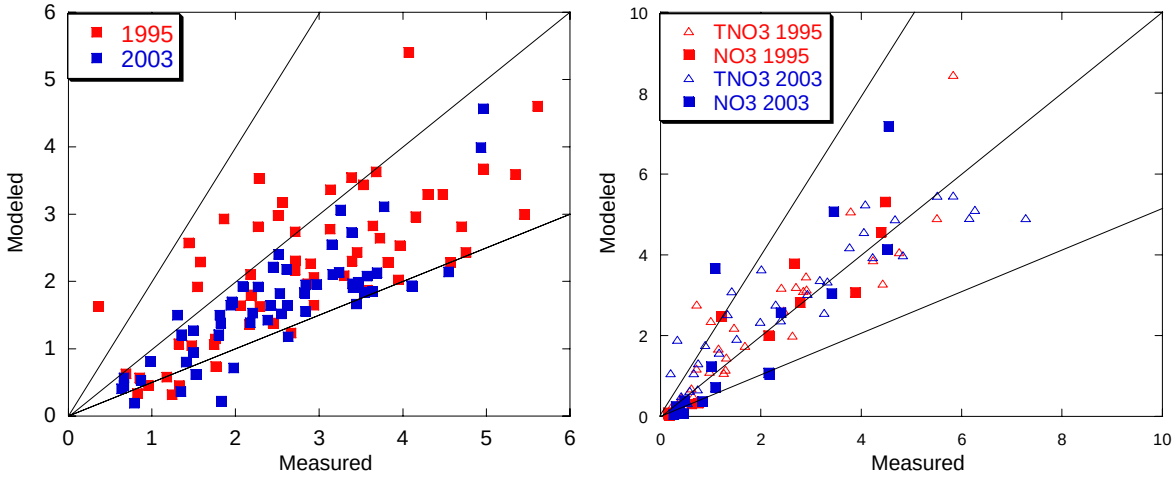

Figure 7.3 Model to measurement (EMEP) comparison for 1995 and 2003, for the sulphate (left) and for nitrate and total nitrate (right). Concentrations are shown in µg/m^3.

8. Discussion and conclusions

Validation of AATSR by comparison to AERONET and MODIS
In this study, a one-year dataset of AATSR aerosol optical thickness data over Europe has been processed for the first time. Because of the large data volume, it was decided to make the cloud detection part of the algorithm fully automatic. However, without rigorous cloud-screening, the large scale distribution of AOT from AATSR in 2003 appeared to be unrealistic. Also, large point sources or source areas such as major cities and even larger scale hot-spot regions could barely be detected. Comparison with MODIS yearly average AOT in 2003, as well as ATSR-2 data revealed large differences in spatial distribution of the AOT.

Therefore, in the project, much emphasis has been on the validation of AATSR data with independent AERONET observations, and the comparison with MODIS. It was found that time correlation between AERONET and AATSR, averaged over all stations, was 0.53 (0.59 median), while it was 0.65 (0.73 median) using MODIS data. Largest errors in AATSR were found in Northern and Eastern Europe, and are likely related to undetected clouds or insufficient surface correction in cases with snow or ice cover. The spatial correlation between yearly average AOT values from AATSR and AERONET was much lower than that using MODIS data. The validation also showed that AATSR has almost no bias, while MODIS did show a significant bias against AERONET. However, it was shown in the PARMA study that the bias in MODIS has a clear seasonality, and could be largely corrected for in a straightforward manner.

It was demonstrated that about 50% of the AATSR data in 2003 needs to be discarded from further use because of potential contamination by clouds or by insufficient surface correction in cases with snow or ice cover. For MODIS about 33% of the data is potentially contaminated by clouds or snow. In the case of AATSR, contamination of the retrieved AOT by clouds and snow-coverage is the dominating source of error. Clearly, detection of clouds and snow-coverage needs to be improved before the AATSR retrieval method can be used in a non-supervised mode for air quality studies in Europe. The quality of the AATSR derived AOT values is not limited because of the accuracy of the level-1 (radiance) data, but is due to shortcomings in the level 1-2 processing (radiances to AOT). Because of this, and also because of the intrinsic advantage of AATSR of having a dual view capability, the improvement of the AOT algorithm might lead to AOT data that are of practical use for air quality studies. Also it is noted that the MODIS algorithm can also be further improved, particularly regarding assumptions on the spectral dependence of the surface reflectance and cloud detection.

Besides the lower accuracy of AATSR as compared to MODIS, also the number of AATSR observations is much more limited because of the small swath, leading to about one observation every three days at maximum in Europe. It turns out that in practice about 65 AATSR observations are available per year for a given location, while MODIS (Terra and Aqua combined) has about 240 observations per year for a given location.

Results of the $PM_{2.5}$ mapping experiments
In an attempt to avoid the large problems with cloud (and snow/ice) contamination in the AATSR data, a selection criterion was used for additional cloud-screening, based on monthly

average data. These screened data were used in the statistical mapping approach. Visual inspection shows that this leads to a better performance for Northern Europe and better agreement with the PARMA study. In the assimilation approach used to map $PM_{2.5}$, instantaneous data are used and a similar cloud-screening method was not possible. Therefore we have used the MODIS cloud-detection in an attempt to avoid cloud contamination in AATSR.

The spatial correlation coefficient between the yearly AOT retrieved from AATSR and the yearly average AOT_F from MODIS is 0.58, after additional cloud-screening of the AATSR data. This indicates that these satellite instruments still show substantial differences in aerosol optical thickness distributions. Since the statistical mapping results are based on both model calculations and measurements, the resulting $PM_{2.5}$ maps based on AATSR and MODIS differs less than the AOT fields. Therefore, the results of the statistical mapping approach were to some extent comparable to MODIS, after application of a additional cloud-screening of the AATSR data. However, there are reasons suggesting that the MODIS based map, resulting from the PARMA study, is more realistic than the map based on AATSR, presented in this report. Firstly, bias-corrected MODIS data show a better comparison with independent AOT measurements from AERONET, as compared to AATSR versus AERONET. Secondly, the fitted $PM_{2.5}$ map based on MODIS exhibits smaller residuals when compared to $PM_{2.5}$ measurements from AirBase. Thirdly, the MODIS results are less sensitive to more-or-less arbitrary methodological choices. Similar to the conclusion of the PARMA study, the assimilation leads to higher $PM_{2.5}$ concentrations, as the model underestimates the AOT. For a discussion on these issues we refer to the PARMA report. However, the small amount of AATSR data for June and July 2003 has led to a limited influence of the AATSR data on the modelled $PM_{2.5}$ fields. In other words, the AATSR data do not strongly constrain the model in the assimilation.

Radiative forcing by nitrate compared to sulphate

Based on our simulations for 2003, the annual radiative forcing by nitrate is calculated to be in the order of 55% of that by sulphate, whereas for 1995 the percentage was only 20%. In summer, nitrate is found to be only regionally important, e.g. in Northwestern Europe, where the forcing of nitrate equals that by sulphate. In winter the nitrate forcing over Europe is about equal to the sulphate forcing. These results are in agreement with estimates based on measured data (Ten Brink et al., 1997; Schaap et al., 2002). Overall, nitrate forcing is significant and gaining importance compared to sulphate and should thus be taken into account to estimate the impact of regional climate change in Europe.

Observation strategy

During the course of the project, the LOTOS-EUROS model has been adapted such that at present, the system is able to simulate on resolutions ranging from 1.0x0.5 degree (50x50km^2) to 0.125x0.0625 degree (6x6 km^2). Also, high-resolution land-use maps were incorporated. The modelling and data-assimilation system developed in the PARMA and HIRAM projects has been applied in what is to our knowledge the first observation system simulation experiment (OSSE) applied to aerosols. In the project 'The operational use of satellite derived aerosol information to assess fine particulate matter concentrations over Europe' which was performed under contract for EUMETSAT, the LOTOS-EUROS model was run in a zoom mode at a resolution of 0.125° x 0.0625°, which corresponds to a horizontal resolution of ~6x6 km^2 (Timmermans et al., 2006). The results indicate that assimilation of simulated AOT at horizontal resolution of 25x25km^2 from two possible future instruments (a Flexible Combined Imager (FCI) instrument providing total AOT and an

Oxygen A-band Sounder instrument providing vertically resolved AOT) improves the analysis and forecast of $PM_{2.5}$ concentrations The level of improvement depends on, among others, the vicinity of simultaneously assimilated ground based measurements and the resolution of the assimilated satellite AOT measurement (temporal resolution between one to four hours). The improvement found in this study is between 20 and 50%.

Cost-benefit analysis

The cost-benefit analysis of this study is essentially the same as that in the PARMA study, with the only important difference that AATSR data are not freely available to end-users, while MODIS data are available for end-users at zero costs, while the quality of AATSR data – at least for 2003 – has proven to be less than that of MODIS. The cost of processing of one year of AATSR satellite data of aerosol optical thickness amounts to about 60.000 Euro, excluding quality control and validation, but including processing of level-two to level-three data (i.e., processing individual AOT images to monthly gridded averages) and improvement of the retrieval algorithm. In the future the algorithm improvement will not be necessary and only running and data processing cost should be considered which can be significantly less than quoted above. From the end-user perspective, data acquisition costs make an important share of total project costs, but the validation and analysis still dominate total project costs. The benefits of using satellite data are improved maps of $PM_{2.5}$ and improved insight in the quality of measuring and modelling AOT and $PM_{2.5}$.

References

- Adams, P.J., J.H. Seinfeld, D. Koch, L. Mickley, and D. Jacob, 2001. General circulation model assessment of direct radiative forcing by the sulfate-nitrate-ammonium-water inorganic aerosol system, J. Geophys. Res., 106(D1), 1097–1112.
- Adelman, Z.E., 1999. A re-evaluation of the Carbon Bond-IV photochemical mechanism. M.Sc. thesis, Department of Environmental Sciences and Engineering, School of Public Health, University of North Carolina, USA.
- Banic, C.M., W.R. Leaitch, G.A. Isaac, M.D. Couture, L.I. Kleinman, S.R. Springston, and J.I. MacPherson, 1996. Transport of ozone and sulfur to the North Atlantic atmosphere during the North Atlantic Regional Experiment. J. Geophys. Res. 101, D22, 29091-29104
- Brunekreef B. and Holgate, S.T., 2002. Air pollution and health. The Lancet 360, 1233-1242.
- Buijsman, E. en F.A.A.M. De Leeuw, 2004. PM_{10} measurement results and correction factors in AirBase, ETC/ACC Technical Paper 2004/4, European Topic Centre on Air and Climate Change, Bilthoven.
- Builtjes P.J.H., van Loon M., Schaap M., Teeuwisse S., Visschedijnk A.J.H., Bloos J.P., 2003. Project on the modelling and verification of ozone reduction strategies: contribution of TNO-MEP, TNO-report MEP-R2003/166, TNO, Apeldoorn.
- Builtjes, P.J.H., H.M. ten Brink, G. de Leeuw, M. van Loon, C. Robles González, M. Schaap, 2001. Aerosol air quality satellite data, BCRS USP-2 report 00-33, Apeldoorn.
- CAFE-Working Group on Particulate Matter, 2004. Second Position Paper on Particulate Matter. See http://europa.eu.int/comm/environment/air/cafe/.
- Charlson, R.J., Schwartz, S.E., Hales, J.M., Cess, R.D., Coakley, J.A., Hansen , J.E., Hofmann, D.J., 1992. Climate forcing by anthropogenic aerosols, Science, 255, 423-430.
- Charron, A., R.M. Harrison, S. Moorcroft, J. Booker, 2004. Quantitative interpretation of divergence between PM_{10} and $PM_{2.5}$ mass measurement by TEOM and gravimetric (Partisol) instruments, Atmos. Env., 38, 415-423.
- Chu, D.A., Y. J. Kaufman, C. Ichoku, L.A. Remer, D. Tanré and B.N. Holben, 2002. Validation of MODIS aerosol optical thickness retrieval over land, Geophys. Res. Lett., 29, NO. 12, doi:10.1029/2001GL013205.
- Chu, D.A., Y.J. Kaufman , G. Zibordi, J.D. Chern, J. Mao, C. Li, and B.N. Holben, 2003. Global monitoring of air pollution over land from the Earth Observing System-Terra Moderate Resolution Imaging Spectroradiometer (MODIS), J. Geophys. Res., 108, 4661, doi:10.1029/2002JD003179.
- Day, D.E. and W.C. Malm, 2001. Aerosol light scattering measurements as a function of relative humidity: a comparison between measurements made at three different sites, Atmos. Env., 35, 5169-5176.
- De Boer, M., De Vente, J., Mücher, C.A., Nijenhuis, W. and Thunnissen, H.A.M., An approach towards pan-European land cover classification and change detection, NRSP-2 Report 00-18, Delft, 110 pp, 2000.
- Dockery D.W., Pope III, C.A., Xu, X., Spengler, J.D., Ware, J. H., Fay, M.E., Ferris, B.G. and Speizer, F.E., 1993. An Association between Air Pollution and Mortality in Six U.S. Cities. The New England Journal of Medicine 329, 1753-1759.

- Eck, T. F., B. N. Holben, J. S. Reid, O. Dubovik, A. Smirnov, N. T. O'Neill, I. Slutsker, and S. Kinne, 1999. Wavelength dependence of the optical thickness of biomass burning, urban, and desert dust aerosols, J. Geophys. Res., 104, 31,333– 31,349.
- EEA, 2000. Documentation about the Corine landcover 2000 dataset is available from: http://reports.eea.europa.eu/COR0-landcover.
- EEA, 2004. EEA Signals 2004, A European Environment Agency update on selected issues, European Environment Agency, Copenhagen.
- EN 12341, 1998. Air Quality – Determination of the PM_{10} fraction of suspended particular matter – Reference method and field test procedure to demonstrate equivalence of measurement methods.
- Engel-Cox, J.A., Holloman, C.H., Coutant, B.W. and Hoff, R.M., 2004. Qualitative and quantitative evaluation of MODIS satellite sensor data for regional and urban scale air quality, Atmospheric Environment 38, 2495-2509.
- Erisman, J.W., van Pul, A., Wyers, P., 1994. Parametrization of surface-resistance for the quantification of atmospheric deposition of acidifying pollutants and ozone, Atmos. Environ., 28, 2595-2607
- EU, 1996. Council Directive 96/62/EC of 27 September 1996 on ambient air quality assessment and management. Official Journal L 296 , 21/11/1996.
- EU, 1999. Council Directive 1999/30/EC of 22 April 1999 relating to limit values for sulphur dioxide, nitrogen dioxide and oxides of nitrogen, particulate matter and lead in ambient air, Official Journal L 163 , 29/06/1999.
- EU, 2005. Thematic strategy on air pollution, COM(2005) 446 final.
- Evensen, G., 1997. Advanced data assimilation for strongly nonlinear dynamics. Monthly Weather Review 125, 1342-1354.
- Flowerdew R. J., and J. D. Haigh, 1995. An approximation to improve accuracy in the derivation of surface reflectances from multi-look satellite radiometers. Geophys. Res. Lett. 23, 1693-1696.
- Hansen J. E. and Sato M., 2001. Trends of measured climate forcings agents, Proc. Nat. Acad. Sci., 98, 14778-14783.
- Henzing, J.S. 2006. Aerosol modelling spatial distributions and effects on radiation, Ph.D thesis Techn.Univ Eindhoven.
- Hitzenberger, R., A. Berner, Z. Galambos, W. Mauenhaut, J. Cafmeyer, J. Schwarz, K. Müller, G. Spindler, W. Wieprecht, K. Acker, R. Hillamo, and T. Mäkelä, 2004. Intercomparison of methods to measure the mass concentration of the atmospheric aerosol during INTERCOMP2000- influence of instrumentation and size cuts, Atmos. Env., 38, 6467-6476.
- Hodzic, A., R.Vautard, H.Chepfer, P. Goloub, L. Menut, P. Chazette, J.L. Deuzé, A. Apituley, and P. Couvert, 2005. Evolution of aerosol optical thickness during the August 2003 heat wave as seen from CHIMERE model simulations and POLDER data, Atmos. Chem. Phys. Discuss, 5, 4115-4141.
- Hutchison, K.D., 2003. Applications of MODIS satellite data and products for monitoring air quality in the state of Texas. Atmospheric Environment 37, 2403-2412.
- Ichoku, C., Remer, L.A., and Eck, T.F., 2005. Quantitative evaluation and intercomparison of morning and afternoon Moderate Resolution Imaging Spectroradiometer (MODIS) aerosol measurements from Terra and Aqua. J. Geophys. Res. 110, D10S03, doi:10.1029/2004JD004987.
- IPCC, 2001. Climate change 2001: The Scientific Basis, Contribution of Working group I to the third assessment report of the IPCC, Houghon et al. (eds), Cambridge, 881 pp.

- Kaufman, Y.J. and D. Tanré, 1998. Algorithm for Remote Sensing of Tropospheric Aerosol from MODIS, Product ID MOD04.
- Kerschbaumer and Reimer, 2003. Meteoroloical data preparation for the Rem/CALGRID model. UBA-projetc 29943246, Freie Univ. Berlin.
- Kiehl, J. T., and B. P. Briegleb, 1993,The relative roles of sulfate aerosols and greenhouse gases in climate forcing, Science, 260, 311-314.
- Kinne S., U. Lohmann, J. Feichter, M. Schulz, C. Timmreck, S. Ghan, R. Easter, M. Chin, P. Ginoux, T. Takemura, I. Tegen, D. Koch, M. Herzog, J. Penner, G. Pitari, B. Holben, T. Eck, A. Smirnov, O. Dubovik, I. Slutsker, D. Tanre, O. Torres, M. Mischenko, I. Geogdzhayev, D.A. Chu, and Y. Kaufman, 2003. Monthly averages of aerosol properties: A global comparison among models, satellite data, and AERONET ground data, J. of Geoph. Res., 108, NO. D20, 4634, doi: 10.1029/2001JD001253.
- Knol A.B. and Staatsen, B.A.M., 2005. Trends in the environmental burden of disease in the Netherlands 1980-2000, RIVM report 500029001, RIVM, Bilthoven.
- Koeble, R. and Seufert G., 2001. Novel maps for forest tree species in Europe, Proceedings of the conference “a changing atmosphere”, Sept 17-20, 2001, Torino, Italy.
- Koelemeijer, R.B.A., P. Stammes, and P.D. Watts, 1998. Comparison of visible calibrations of GOME and ATSR-2, Remote Sensing of the Environment, 63, 279-288.
- Koelemeijer, R.B.A., P. Stammes, J.W. Hovenier, and J.D. de Haan, 2001. A fast method for retrieval of cloud parameters using oxygen-A band measurements from the Global Ozone Measurement Instrument, J. Geophys. Res., 106, pp. 3475-3490.
- Koelemeijer, R.B.A., M. Schaap, R.M.A. Timmermans, C.D. Homan, J. Matthijsen, J. van de Kassteele, P.J.H. Builtjes, 2006a. Mapping aerosol concentrations and optical thickness over Europe – PARMA final report, MNP report 555034001, Bilthoven.
- Koelemeijer, R.B.A., Homan, C.D., and Matthijsen, J., 2006b. Comparison of spatial and temporal variations of aerosol optical thickness and particulate matter in Europe, Atmos. Env., 40, 5304-5315.
- Koepke, P., Hess, M., Schult, I., Shettle, E.P., 1997. Global aerosol data set, Max-Planck Institut für Meteorologie, Report No 243, Hamburg, Germany.
- Liu and Durran, 1977. The development of a regional air pollution model and its application to the Northern Great Planes, EPA-908/1-77-001, p. 281 SAI, San Rafael, California.
- Logan, J., 1998. An analysis of ozonesonde data for the troposphere, recommendations for testing 3-D models and development of a gridded climatology for tropospheric ozone, J. Geophys. Res. 104, 16.
- Matthews, E., 1984. Vegetation, land-use and seasonal albedo data sets: Documentation and archived data tape, NASA Tech. Memo, 86107.
- Mie, G., 1908. Beiträge zur optik trüber medien, speziell kolloidaler metallösungen, Ann. Phys., Leipzig, 25, 377-445.
- Monahan, E.C., Spiel, D.E., Davidson, K.L., 1986. A model of marine aerosol generation via whitecaps and wave disruption, In Oceanic Whitecaps and their role in in air/sea exchange, edited by Monahan, E.C, and Mac Niocaill, G., pp. 167-174, D. Reidel, Norwell, Mass., USA
- Nenes, A., Pilinis, C., and Pandis, S. N., 1999. Continued Development and Testing of a New Thermodynamic Aerosol Module for Urban and Regional Air Quality Models, Atmos. Env. 33, 1553-1560
- Pope III, C.A., Dockery, D.W., Schwartz, J., 1995. Review of epidemiological evidence of health effects of particulate air pollution. Inhalation Toxicology 7, 1–18.

- Pope III, C.A.., Burnett, R.T., Thun, M.J., Calle, E.E., Krewski, D, Ito, K., Thurston, G.D., 2002. Lung Cancer, Cardiopulmonary Mortality, and Long-term Exposure to Fine Particulate Air Pollution, J. Am. Med. Assoc. 287, 1132-1141.
- Poppe, D., Y. Andersson-Sköld, A. Baart, P.J.H. Builtjes, M. Das, F. Fiedler, O. Hov, F. Kirchner, M. Kuhn, P.A. Makar, J.B. Milford, M.G.M. Roemer, R.Ruhnke, D. Simpson, W.R. Stockwell, A. Strand, B. Vogel, H. Vogel, 1996. Gas-phase reactions in atmospheric chemistry and transport models: a model intercomparison. Eurotrac report. ISS, Garmisch-Partenkirchen.
- Remer, L.A., Y.J. Kaufman, D. Tanré, S. Mattoo, D.A. Chu, J.V. Martins, R.-R. Li, C. Ichoku, R.C. Levy, R.G. Kleidman, T.F. Eck, E. Vermote, and B.N. Holben, 2005. The MODIS Aerosol Algorithm, Products, and Validation, J. Atmos. Sci., 62, 947-973.
- Robles González, C., J.P. Veefkind, and G. de Leeuw, 2000. Aerosol optical depth over Europe in August 1997 derived from ATSR-2 data, Geophys. Res. Lett., 27, 955-958.
- Robles González, C., M. Schaap, G. de Leeuw, P.J.H. Builtjes, and M. van Loon, 2003. Spatial variation of aerosol properties over Europe derived from satellite observations and comparison with model calculations, Atmos. Chem. Phys., 3, 521-533.
- Schaap, M., Muller, K., ten Brink, H.M., 2002. Constructing the European aerosol nitrate concentration field from quality analysed data, Atmos. Environ, 36, 1323-1335.
- Schaap M., 2003. On the importance of aerosol nitrate over Europe, PhD-thesis, University of Utrecht.
- Schaap, M., M. van Loon, H.M. ten Brink, F.J. Dentener, and P.J.H. Builtjes, 2004a. Secondary inorganic aerosol simulations for Europe with special attention to nitrate, Atmos. Chem. Phys., 4, 857-874.
- Schaap, M., H.A.C. Dernier Van Der Gon, F.J. Dentener, A.J.H. Visschedijk, M. Van Loon, H.M. Ten Brink, J.-P. Putaud, B. Guillaume, C. Liousse, and P.J.H. Builtjes, 2004b. Antropogenic black carbon and fine aerosol distribution over Europe. J. Geophys. Res. 109, D18207, doi:10.1029/2003JD004330.
- Schaap, M., M. Roemer, F. Sauter, G. Boersen, R. Timmermans, P.J.H. Builtjes, 2005a. LOTOS-EUROS: Documentation, TNO-report B&O-A R 2005/297, TNO, Apeldoorn.
- Schaap, M. Sauter, F., Timmermans, R.M.A., Roemer, M., Velders, G., Beck, J., and Builtjes, P.J.H., 2005b. The LOTOS-EUROS model: description, validation and latest developments, Int. J. of Environment and Pollution, accepted.
- Shettle, E.P. and R.W. Fenn, 1979. Models for the Aerosols of the Lower Atmosphere and the Effects of Humidity Variations on Their Optical Properties, AFGL-TR-79-0214 Environmental Research Papers, #676, published by the Air Force Geophysics Laboratory, Hanscom AFB, MA 01731.
- Simpson, D., H. Fagerli, J.E. Jonson, S. Tsyro, P. Wind, and J-P. Tuovinen, 2003. Transboundary Acidification, Eutrophication and Ground Level Ozone in Europe, Part 1: Unified EMEP Model Description, EMEP Report 1/2003, Norwegian Meteorological Institute, Oslo, Norway.
- Sokolik I. N., O. B. Toon, R. W. Bergstrom, 1998. Modeling the radiative characteristics of airborne mineral aerosols at infrared wavelengths. J. Geophys. Res. 103, 8813-8826.
- Stammes, P., 2001. Manual for the DAK program, Royal Netherlands Meteorological Institute, De Bilt, the Netherlands
- Tang, I. N., 1997. Thermodynamic and optical properties of mixed-salt aerosols of atmospheric importance, J. Geophys. Res., 102, D2, 1883–1893.
- Tegen, I., P. Hollrig, M.Chin, I. Fung, D. Jacob, J. Penner, 1997, Contribution of different aerosol species to the global aerosol extinction optical thickness: Estimates from model results. J. Geophys. Res. 102, 23,895-23,915.

- Ten Brink, H.M, Kruisz, C., Kos, G.P.A., Berner, A., 1997. Composition/size of the light-scattering aerosol in the Netherlands, Atmos. Environ., 31, 3955-3962.
- Ten Brink H. M., Hensen, A., Khystov, A., van Dorland, R., Jeuken, A., van Velthoven, P., Lelieveld, J., van den Berg, A., Swart, D.P.J., Bergwerff, J.B., Apituley, A., 2001. Aerosol; cycle and influence on the radiation balance, Cluster-project in the National Research Program on Global Air Pollution and Climate Change, npr2, ECN report 410200064, ECN, Petten.
- Timmermans, R.M.A., M. Schaap, P.J.H. Builtjes, R. Siddans, 2006. The operational use of satellite derived aerosol information to assess fine particulate matter concentrations over Europe, TNO-report 2006-A-R0309-B, TNO, Apeldoorn.
- Van de Hulst, 1981. Light scattering by small particles, ISBN 0-486-64228-3, Dover Publications, New York.
- Van de Kassteele, J., Koelemeijer, R.B.A., Dekkers, A.L.M., Schaap, M., C. D. Homan, C.D., Stein, A., 2006. Statistical mapping of PM10 concentrations over Western Europe using secondary information from dispersion modelling and MODIS satellite observations, Stochastic Env. Research and Risk Assessment, DOI 10.1007/s00477-006-0055-4.
- Van Donkelaar, A., R.V. Martin, and R.J. Park, 2006. Estimating ground-level $PM_{2.5}$ using aerosol optical depth determined from satellite remote sensing, J. Geophys. Res., 111, doi:10.1029/2005JD006996.
- Van Dorland, R., Dentener, F.J., Lelieveld, J., 1997. Radiative forcing due to tropospheric ozone and sulphate aerosols, J. Geophys. Res., 102, 28079-28100.
- Van Loon, M, P.J.H. Builtjes, A.Segers, 2000. Data assimilation of ozone in the atmospheric transport chemistry model LOTOS, Env. Modelling and Software 15, 603-609.
- Veefkind J.P., J.C.H. van der Hage, and H.M. ten Brink, 1996. Nephelometer derived and directly measured aerosol optical thickness of the atmospheric boundary layer, Atmos. Res., 41, 217-228.
- Veefkind J. P., G. de Leeuw, and P.A. Durkee, 1998a. Retrieval of Aerosol Optical Depth over Land using two angle view Satellite Radiometry during TARFOX, Geophys. Res. Lett., 25, 3135-3138.
- Veefkind J.P. and G. de Leeuw, 1998b. A new algorithm to determine the spectral aerosol optical depth from satellite radiometer measurements, J. Aerosol Sci., 29, 1237-1248.
- Veefkind, J.P., 1999. Aerosol Satellite Remote Sensing. PhD thesis, Utrecht University, Utrecht, the Netherlands.
- Veefkind J.P., G. de Leeuw, P. Stammes, and R.B.A. Koelemeijer, 2000. Regional Distribution of Aerosol over land derived from ATSR-2 and GOME. Remote Sensing of the Environment, 74, 377-386.
- Veldt, C. 1991. The use of biogenic VOC measurements in emission inventories, MT-TNO Report 91-323, TNO, Apeldoorn.
- Verver G.H.L., J.S. Hensing, M. Schaap, P.J.H. Builtjes, P.F.J. Velthoven, R. Schoemaker, G. de Leeuw, 2006. Aerosol Retrieval and Assimilation phase 2 (ARIA-2). NIVR-Rep.
- Visschedijk, A.J.H. and H.A.C. Denier van der Gon, 2005. Gridded European anthropogenic emission data for NOx, SOx, NMVOC, NH3, CO, PM 10, PPM 2.5 and CH4 for the year 2000. TNO-Rep B&O-A R 2005/106, TNO, Apeldoorn.
- Volz, F.E., 1972. Infrared refractive index of atmospheric aerosol substances, Applied Optics, 11, pp. 755-759.

- Walcek,C.J. 2000. Minor flux adjustment near mixing ration extremes for simplified yet highly accurate monotonic calculation of tracer advection. J. Geophys. Res. 105, D7, 9335-9348.
- Wang J. and Christopher, S.A. 2003. Intercomparison between satellite-derived aerosol optical thickness and PM2.5 mass: implications for air quality studies. Geophys. Res. Lett., 30 (21), 2095, doi:10.1029/2003GL018174.
- Whitten G., Hogo, H., Killus, J., 1980. The Carbon Bond Mechanism for photochemical smog, Env. Sci. Techn. 14, 14690-700.
- Yamartino R.J., J. Flemming, R.M. Stern., 2004. Adaption of analytic diffusivity formulation to Eulerian grid model layers of finite thickness, 27th NATO/CCMS ITM on air pollution modelling and its application, Banff.

Appendix A The LOTOS-EUROS model system

A1. Model description

Domain
The master domain of LOTOS-EUROS is bound at 35° and 70° North and 10° West and 60° East. The projection is normal longitude-latitude and the standard grid resolution is 0.50° longitude x 0.25° latitude, approximately 25x25 km^2. In this study we have used several domains within this master domain. The final results are calculated over a domain that covers Europe (up to 40° East) but excludes the largest part of European Russia. In the vertical there are three dynamic layers and an optional surface layer. The model extends in vertical direction 3.5 km above sea level. The lowest dynamic layer is the mixing layer, followed by two reservoir layers. The height of the mixing layer is part of the diagnostic meteorological input data. The heights of the reservoir layers are determined by the difference between the mixing layer height and 3.5 km. Both reservoir layers are equally thick with a minimum of 50m. In some cases when the mixing layer extends near or above 3500 m the top of the model exceeds the 3500 m according to the abovementioned description. Simulations were performed with the optional surface layer of a fixed thickness of 25 m. Hence, this layer is always part of the dynamic mixing layer. For output purposes the concentrations at measuring height (usually 3.6 m) are diagnosed by assuming that the flux is constant with height and equal to the deposition velocity times the concentration at height z.

Transport
The transport consists of advection in three dimensions, horizontal and vertical diffusion, and entrainment/detrainment. The advection is driven by meteorological fields (u, v) which are input every 3 hours. The vertical wind speed w is calculated by the model as a result of the divergence of the horizontal wind fields. The recently improved and highly-accurate, monotonic advection scheme developed by Walcek (2000) is used to solve the system. The number of steps within the advection scheme is chosen such that the courant restriction is fulfilled. Entrainment is caused by the growth of the mixing layer during the day. Each hour the vertical structure of the model is adjusted to the new mixing layer thickness. After the new structure is set the pollutant concentrations are redistributed using linear interpolation.
The horizontal diffusion is described with a horizontal eddy diffusion coefficient following the approach by Liu and Durran (1977). Vertical diffusion is described using the standard Kz-theory. Vertical exchange is calculated employing the new integral scheme by Yamartino et al. (2004).

Chemistry
The LOTOS-EUROS model contains two chemical mechanisms, the TNO CBM-IV scheme (Schaap et al., 2005a) and the CBM-IV by Adelman (1999). In this study we used the TNO CBM-IV scheme which is a modified version of the original CBM-IV (Whitten et al., 1980). The scheme includes 28 species and 66 reactions, including 12 photolytic reactions. Compared to the original scheme steady state approximations were used to reduce the number of reactions. In addition, reaction rates have been updated regularly. The mechanism was tested against the results of an intercomparison presented by Poppe et al. (1996) and found to be in good agreement with the results presented for the other mechanisms. Aerosol chemistry is represented using ISORROPIA (Nenes et al., 1999).

Dry and wet deposition
The dry deposition in LOTOS-EUROS is parameterised following the well known resistance approach. The deposition velocity is described as the reciprocal sum of three resistances: the aerodynamic resistance, the laminar layer resistance and the surface resistance. The aerodynamic resistance is dependent on atmospheric stability. The relevant stability parameters (u*, L and Kz) are calculated using standard similarity theory profiles. The laminar layer resistance and the surface resistances for acidifying components and particles are described following the EDACS system (Erisman et al., 1994).

Below cloud scavenging is described using simple scavenging coefficients for gases (Schaap et al., 2004) and following Simpson et al. (2003) for particles. In-cloud scavenging is neglected due to the limited information on clouds. Neglecting in-cloud scavenging results in too low wet deposition fluxes but has a very limited influence on ground level concentrations (see Schaap et al., 2004a).

Meteorological input
The LOTOS-EUROS system is presently driven by 3-hourly meteorological data. These include 3D fields for wind direction, wind speed, temperature, humidity and density, substantiated by 2-d gridded fields of mixing layer height, precipitation rates, cloud cover and several boundary layer and surface variables. The standard meteorological data for Europe are produced at the Free University of Berlin employing a diagnostic meteorological analysis system based on an optimum interpolation procedure on isentropic surfaces. The system utilizes all available synoptic surface and upper air data (Kerschbaumer and Reimer, 2003). Also, meteorological data obtained from ECMWF can be used to force the model.

Emissions
The anthropogenic emissions used in this study are a combination of the TNO emission database (Visschedijk and Denier van der Gon et al., 2005) and the CAFE baseline emissions for 2000. For each source category and each country, we have scaled the country totals of the TNO emission database to those of the CAFE baseline emissions. Elemental carbon (EC) emissions were derived from (and subtracted from) the primary $PM_{2.5}$ ($PPM_{2.5}$) emissions following Schaap et al. (2004b). Hence, we use the official emission totals as used within the LRTAP protocol but we benefit from the higher resolution of the TNO emission database (0.25x0.125 lon-lat). The annual emission totals are broken down to hourly emission estimates using time factors for the emissions strength variation over the months, days of the week and the hours of the day (Builtjes et al., 2003).

In LOTOS-EUROS biogenic isoprene emissions are calculated following Veldt (1991) using the actual meteorological data. In addition, sea salt emissions are parameterised following Monahan et al. (1986) from the wind speed at ten meter height. Dust was neglected as it normally does not contribute a large fraction to the fine aerosol mass in Europe and, more importantly, because there are no reliable emission estimates and/or parameterisations

Boundary conditions
The boundary conditions for ozone are derived from the 3-D climatological dataset by Logan (1998), which is derived from ozone sonde data. For a number of components, listed in Table A.1 we follow the EMEP method (Simpson et al., 2003) based on measured data. In this method simple functions have been derived to match the observed distributions. The boundary conditions are adjusted as function of height, latitude and day of the year. The functions are used to set the boundary conditions, both at the lateral boundaries as at the

model top. The annual cycle of each species is represented with a cosine-curve, using the annual mean near-surface concentration, C_0, the amplitude of the cycle ΔC, and the day of the year at which the maximum value occurs, d_{max}. Table A.1 lists these parameters.

We first calculate the seasonal changes in ground-level boundary condition, C_0, through:

$$C_0 = C_{mean} + \Delta C \cdot \cos\left(2\pi \frac{(d_{mm} - d_{\max})}{n_y}\right)$$

where n_y is the number of days per year, d_{mm} is the day number of mid-month (assumed to be the 15th), and d_{max} is day number at which C_0 maximises, as given in Table A.1. Changes in the vertical are specified with a scale-height, H_z, also given in Table A.1.

$$C_i(h) = C_0 e^{-\frac{h}{Hz}}$$

where $C_i(h)$ is the concentration at height h (in km). For simplicity we set h to be the height of the centre of each model layer assuming a standard atmosphere. For some species a latitude factor, given in Table A.2, is also applied. Values of C_i adjusted in this manner are constrained to be greater or equal to the minimum values, C_{min}, given in Table A.1. Ammonia boundary conditions are neglected. Sulphate is assumed to be fully neutralised by ammonium. Nitrate values are assumed to be included in those of nitric acid and are zero as well.

Table A.1 Parameters used to set the boundary conditions.

Parameter	C_{mean}	d_{max}	ΔC	*Hz*	$C_0^{\min}$	$C_h^{\min}$
	ppb	days	ppb	km	ppb	ppb
SO_2	0.15	15.0	0.05	∞	0.15	0.03
SO_4	0.15	180.0	0.00	1.6	0.05	0.03
NO	0.1	15.0	0.03	4.0	0.03	0.02
NO_2	0.1	15.0	0.03	4.0	0.05	0.04
PAN	0.20	120.0	0.15	∞	0.20	0.1
HNO_3	0.1	15.0	0.03	∞	0.05	0.05
CO	125.0	75.0	35.0	25.0	70.0	30.0
ETH	2.0	75.0	1.0	10.0	0.05	0.05
FORM	0.7	180.0	0.3	6.0	0.05	0.05
ACET	2.0	180.0	0.5	6.0	0.05	0.05

Table A.2 Latitude factors applied to the prescribed boundary conditions.

Component	Latitude (°N)							
	35	40	45	50	55	60	65	70
SO_2, SO_4, NO, NO_2	0.15	0.3	0.8	1.0	0.6	0.2	0.12	0.05
HNO_3, FORM, ACET	1.0	1.0	0.85	0.7	0.55	0.4	0.3	0.2
PAN	0.33	0.5	0.8	1.0	0.75	0.5	0.3	0.1
CO	0.7	0.8	0.9	1.0	1.0	0.95	0.85	0.8

AOT calculation

The AOT is computed from the dry aerosol mass concentrations derived from the LOTOS-EUROS model using the approach of Kiehl and Briegleb (1993):

$$AOT_i(\lambda) = f(RH, \lambda) * a_i(\lambda) * B_i(\lambda)$$

where $a_i(\lambda)$ is the mass extinction efficiency of the compound i; B_i is the column burden of the compound i; f (RH, λ) is a function describing the variation of the scattering coefficient with relative humidity (RH) and wavelength (l). To compute $a_i(\lambda)$ for dry inorganic particles, a Mie (Mie, 1908) code has been used, assuming the aerosol size distribution to be log-normal, with a geometric mean radius of 0.05μm, a geometric standard deviation of 2.0 and a sulphate dry particle density of 1.7 g cm^{-3} (Kiehl and Briegleb, 1993). Most aerosol particles absorb or release water vapour when the relative humidity (RH) changes. Thus the size and composition of the particles change, resulting in different light scattering properties. To account for the variation of the aerosol scattering coefficient with RH, the factor f(RH, λ), derived from humidity controlled nephelometry (Veefkind et al., 1996), is used (see Figure A.1). Similar functions for f(RH) have been reported by Day and Malm (2001) for various locations in the United States. Effects due to hysteresis (e.g. Tang, 1997) are not accounted for. The wavelength dependence of f (RH) can be ignored (Veefkind et al., 1999). The scattering calculations were made with RH values taken from the analysed meteorological data file that is used as input to the LOTOS-EUROS model, including the variations of RH with height. For the organic aerosol components we have used an a_i of 9 for EC and 7 for OC (Tegen et al., 1997). For these components the growth as function of RH has been neglected.

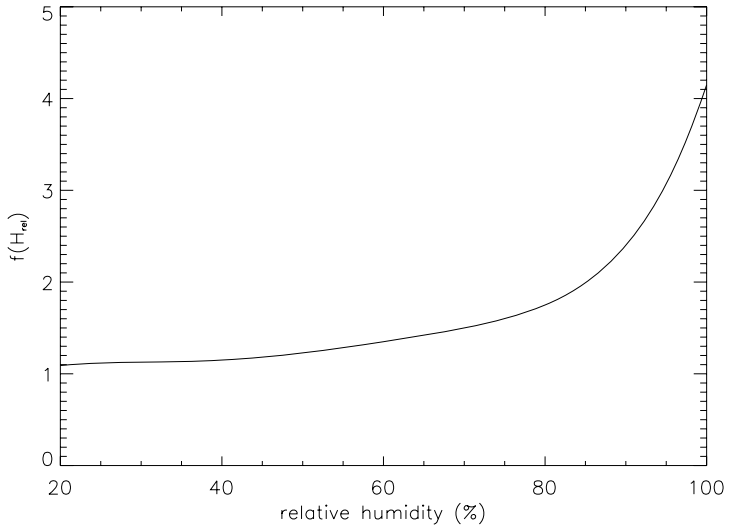

Figure A.1 Function f(RH) that describes the increase of extinction efficiency (or cross-section) with increasing relative humidity (based on Veefkind et al., 1996).

A2. Data assimilation system of LOTOS-EUROS

The first step in order to build the Ensemble Kalman Filter around LOTOS-EUROS is to embed the model and the available measurement in a stochastic environment:

$$x^{k+1} = f^k(x^k, w^k)$$
$$y^k = C^k x^k + v^k,$$

where the superscripts (k) denote the time-steps. The model state vector is denoted by *x* and the measurements by *y*. The function *f* denotes the non-linear model operator which apart from on the state vector acts on a white noise vector *w* with Gaussian distribution and diagonal covariance matrix *Q*. The measurement vector *y* is assumed be a linear combination of elements of the state vector and a random, uncorrelated Gaussian error *v* with (diagonal) covariance matrix *R*. The basic idea behind the ensemble filter is to express the probability function of the state in an ensemble of possible states $\{\xi_1,..., \xi_N\}$, and to approximate statistical moments with sample statistics:

$$\hat{x} \approx \frac{1}{N}\sum_{j=1}^{N} \xi_j$$
$$P \approx \frac{1}{N-1}\sum_{j=1}^{N} \left(\xi_j - \hat{x}\right)\left(\xi_j - \hat{x}\right)^T$$

where the pair ($\hat{x}$,*P*) (expectation and covariance matrix) describe the probability of the state vector *x* completely if *x* has a Gaussian distribution. Since we are dealing with strongly non-linear models, it cannot be expected that *x* really has a Gaussian distribution. We assume however that the distribution is at least close to Gaussian so that the bulk of the statistical properties is captured by the pair ($\hat{x}$,*P*). The filter algorithm consists of three stages:

<u>initialisation</u>:
each ensemble member is set to the initial state:

$$\xi_j = x^0$$

<u>forecast</u>:
each ensemble member is propagated in time by the model, where the noise input w^k is drawn from a random generator with covariance Q;

$$\xi_j^f = f(\xi_j, w^k)$$

<u>analysis</u>:
given an (arbitrary) gain matrix K, each ensemble member is updated according to:

$$\xi_j^a = \xi_j^f + K(y + v - H^T \xi_j^f)$$

where v_j represents a measurement error, drawn from a random generator with zero mean and covariance *R*. The gain matrix *K* is given by the optimal gain matrix from the original Kalman Filter. In the original filter the Kalman gain was obtained by matrix multiplications

in which the covariance matrix P is involved. Fortunately, the use of this matrix can be avoided, since this matrix is too large to store into memory. Instead, a square root S (such that $P=SS^T$) can be used. From the definition of P it can be seen that the columns s_i of such a square root can be defined by

$$s_i = \frac{1}{\sqrt{N-1}}\left(\xi_i - \hat{x}\right).$$

Note that the sample mean $\hat{x}$, and the matrix S completely define the ensemble and vice versa; it is therefore not necessary to store both S and the ensemble. The analysis of the measurements y_j (entries of the vector y) can now be performed by the following sequential procedure (dropping the time index):

$$h_j = S_{j-1}^T c_j^T$$
$$a_j = \left(h_j^T h_j + r_{jj}\right)^{-1}$$
$$b_j = \left(1 + \sqrt{a_j r_{jj}}\right)^{-1}$$
$$k_j = a_j S_{j-1} h_j$$
$$S_j = S_{j-1} - b_j k_j h_j^T$$
$$x_j = x_{j-1} + h_j\left(y_j - c_j x_{j-1}\right)$$

The index j is the iteration index. The starting values for the procedure are $S_0 = S_f^{k+1}$ and $x_0 = x_f^{k+1}$.
After the analysis of all the measurements the final values for the state vector and (square root of) the covariance matrix have been obtained: $S^{k+1} = S_m$ and $x^{k+1} = x_m$. For a detailed description we refer to Van Loon et al. (2000) and Evensen (1997). The forecast step is the most expensive part of the algorithm, since for each ensemble member the model has to be evaluated one time. Typical ensemble sizes range from 10-100. If the number of measurements is limited (in order of hundreds), the total computation time involved with the ensemble filter is proportional with the ensemble size.

Random noise

In the model implementation used in this study, the noise parameters are part of the model state. Hence they are estimated by the filter as well. Noise is applied to several emission fields E_j and deposition rates. The noise parameters w_i can be interpreted as emission correction factors since the actual emission field E_j is estimated by the filter as

$$E_i \leftarrow E_j\,(1+w_i).$$

This approach has the disadvantage that there is no 'memory' in the system: the w_i are uncorrelated in time; at a certain hour t the noise parameter may indicate an emission increase of 20% with respect to the original field, whereas it estimates a decrease of 20% at $t+1$. Such irregular behaviour can be prevented to a large extent by the use of coloured noise. However, in the present set-up we use the same noise factors for the 24 hour period between overpasses. Hence, the long period between the measurements warrants some correlation in time.

Spatially limiting influence of measurements

For two reasons correlations between elements in the state vector arise which are unlikely to be correlated. Firstly, spurious correlations arise, mainly because the sample size is finite. Secondly, undesired correlations arise due to the choice of the noise processes. The noise processes to be introduced in this study are all acting on emission fields of various emitted compounds causing 'instantaneous' correlations throughout the domain. For example the particulate matter concentration at hour *t* somewhere in the Netherlands becomes correlated with the particulate matter concentration in, say, the south of France, because noise was added to the NO_x emission field at hour *t*-1. Although this is exactly what should happen when defining noise in this way, such correlations are not realistic and should be somehow ignored by the filter. The noise processes is chosen this way because it is infeasible to subdivide the emission fields into a number of sub-domains on each of which a different noise parameter is acting. That would increase the dimension of the noise vector dramatically and hence the necessary ensemble size to capture the statistical properties.

One way to ignore unrealistic correlations over large distances is the use of a gain matrix which is only unequal to zero around the locations of observations. Such a gain matrix k may be formed using a covariance matrix which is an element wise product of the original sample covariance and a correlation function with local support. For a single scalar measurement, the resulting gain matrix is given by (omitting the subscripts):

$$k = I(\rho)Ph/(h^T Ph + r)$$

where $I(\rho)$ is a diagonal matrix; the diagonal elements are filled with a prescribed correlation between the corresponding grid cell and the grid cell of the measurement. Different choices for the values of ρ_i are possible. In this study we take

$$\rho_i = \exp(-0.5\ (r_i/L)^2) \quad \text{for } r_i \leq 3.5\ L$$

and zero otherwise. r_i denotes the distance from the grid cell considered to the site of the analysed measurement and *L* denotes a length scale parameter, taken to be 100 km in this study.